

NASA  
Contractor Report 4771

Army Research Laboratory  
Contractor Report ARL-CR-339

# New Methods for Improved Double Circular-Arc Helical Gears

Faydor L. Litvin and Jian Lu  
*University of Illinois at Chicago*  
*Chicago, Illinois*

Prepared for  
U.S. Army Research Laboratory  
and  
Lewis Research Center  
under Grant NAG3-1607



National Aeronautics and  
Space Administration

**Office of Management**  
Scientific and Technical  
Information Program

**1997**



# Contents

<b>Chapter 1 Introduction</b> .....	1
<b>Chapter 2 Basic Principles of Generation of Double Circular-Arc Helical Gears</b> .....	3
2.1 Generation of External Gears .....	3
2.1.1 Principle of Generation .....	3
2.1.2 Geometry of Rack-Cutter .....	5
2.1.3 Equation of Meshing Between Rack-Cutter and Gear Surfaces .....	7
2.2 Geometry of External Gears .....	8
2.3 Generation of Internal Gears .....	11
2.4 Geometry of Internal Gears .....	12
<b>Chapter 3 Computerized Simulation of Meshing for Double Circular-Arc Helical Gears</b> .....	15
3.1 Computerized Simulation of Meshing and Contact .....	15
3.2 Numerical Examples .....	18
3.2.1 Example 1 (External Gear Drive) .....	18
3.2.2 Example 2 (Internal Gear Drive) .....	19
3.2. Example 3 .....	20
<b>Chapter 4 Generation of Double Circular-Arc Helical Gears by Grinding Disks</b> .....	21
4.1 Computerized Design of the Grinding Disks .....	21
4.2 Generation of Gear (Pinion) Tooth Surface $S_i$ by Grinding Disk $S_t$ .....	25
<b>Chapter 5 Generation of Gear Drive With Low Transmission Errors by Application of Imaginary Rack-Cutters</b> .....	29
5.1 Basic Principle .....	29
5.2 Equation of Meshing .....	30
5.3 Modified Pinion Tooth Surface .....	32
5.4 Simulation of Meshing .....	33
<b>Chapter 6 Generation of Modified Pinion by Worms</b> .....	35
6.1 Introduction .....	35
6.2 Determination of Worm Thread Surface $S_w$ Generated by Rack-Cutter Surface $S_P$ .....	35
6.3 Generation of Pinion Tooth Surface by Worm .....	41
<b>Chapter 7 Directions for Users of Application of Computer Programs</b> .....	45
7.1 Program 1: Design of External Gear Drive .....	45
7.1.1 Name of the Program .....	45
7.1.2 Function of the Program .....	45
7.1.3 Input Data File 90 .....	45
7.1.4 Running the Program .....	46
7.1.5 Output Data Files .....	46

7.2 Program 2: Design of Internal Gear Drive .....	48
7.2.1 Name of the Program .....	48
7.2.2 Function of the Program .....	48
7.2.3 Input Data File 90 .....	49
7.2.4 Running the Program .....	49
7.2.5 Output Data Files .....	49
7.3 Program 3: Design of Grinding Disk .....	50
7.3.1 Name of the Program .....	50
7.3.2 Function of the Program .....	51
7.3.3 Input Data File 91 .....	51
7.3.4 Running the Program .....	51
7.3.5 Output Data Files .....	52
7.4 Program 4: Design of Grinding Worm .....	52
7.4.1 Name of the Program .....	52
7.4.2 Function of the Program .....	52
7.4.3 Input Data File 90 .....	52
7.4.4 Running the Program .....	53
7.4.5 Output Data Files .....	53
References .....	53

# Chapter 1

## Introduction

Circular arc helical gears were proposed by Wildhaber and Novikov. However, there is a significant difference between the ideas proposed by the previously mentioned inventors. Wildhaber's idea (ref. 1) is based on generation of the pinion and gear by the same imaginary rack-cutter that provides conjugate gear tooth surfaces that are in *line* contact at every instant. Novikov (ref. 2) proposed the application of two mismatched imaginary rack-cutters that provide conjugated gear tooth surfaces that are in point contact at every instant. This allowed us to overcome the restriction caused by the relation between the curvatures of surfaces that are in line contact and to obtain a small value of the relative normal curvature of the contacting surfaces. Novikov's approach enables us to reduce the contact stresses.

The weak point of Novikov's idea was the high value of bending stresses caused by the instantaneous point contact of gear tooth surfaces. This disadvantage could be overcome by the development of double circular-arc helical gears with two zones of meshing. The geometry of Novikov helical gears was considered in references 3 to 8.

The content of this report covers the following main topics:

- (1) The geometry of double circular-arc helical pinion and gear applied in external and internal gear drives
- (2) New methods for generation of the aforementioned gear drives with a low level of transmission errors
- (3) Methods of grinding of double circular-arc pinion and gear
- (4) Computerized simulation of meshing and contact of the previously discussed gear drives

Computer programs for numerical computation were developed for all stages of investigation. The results of computation confirm that the transmission errors of Novikov's helical gears are impermissibly high and the function of transmission errors is a discontinuous one. The results of computation confirm as well that the proposed modification of surfaces and methods for generation allows us to reduce the level of transmission errors in two times and substitute the discontinuous function of transmission errors by the continuous one of a parabolic type.



# Chapter 2

## Basic Principles of Generation of Double Circular-Arc Helical Gears

### 2.1 Generation of External Gears

#### 2.1.1 Principle of Generation

The imaginary process for external gear generation is based on the following ideas:

- (1) Two imaginary rack-cutters with cylindrical surfaces  $\Sigma_p$  and  $\Sigma_f$  are rigidly connected each to other as shown in figure 1(a). Surfaces  $\Sigma_p$  and  $\Sigma_f$  are in tangency along two straight lines,  $a - a$  and  $b - b$ .
- (2) The rack-cutters perform translational motion with velocity  $v$  while the pinion and gear being generated perform rotational motions about their axes,  $O_1$  and  $O_2$ , with angular velocities  $\omega^{(1)}$  and  $\omega^{(2)}$  (fig. 1(b)). The axodes of the gears are cylinders of radii  $r_1$  and  $r_2$ , where  $r_i = v/\omega^{(i)}$  ( $i = 1, 2$ ). Both rack-cutters have the same axode, that is, plane  $\Pi$  (fig. 1(a)).
- (3) The rack-cutter surface  $\Sigma_p$  generates the pinion tooth surface  $\Sigma_1$  only, and the rack-cutter surface  $\Sigma_f$  generates only the gear tooth surface  $\Sigma_2$ . Surface  $\Sigma_1$  is the envelope to the family of rack-cutter surfaces  $\Sigma_p$  that are represented in coordinate system  $S_1$ . Similarly, surface  $\Sigma_2$  is the envelope to the family of rack-cutter surfaces  $\Sigma_f$  that are represented in coordinate system  $S_2$ .
- (4) We may consider four surfaces ( $\Sigma_p$ ,  $\Sigma_1$ ,  $\Sigma_f$  and  $\Sigma_2$ ) that are in mesh simultaneously. Surfaces  $\Sigma_p$  and  $\Sigma_1$  are in contact along two lines at every instant. Similarly, surfaces  $\Sigma_f$  and  $\Sigma_2$  are in contact at two lines at every instant as well.

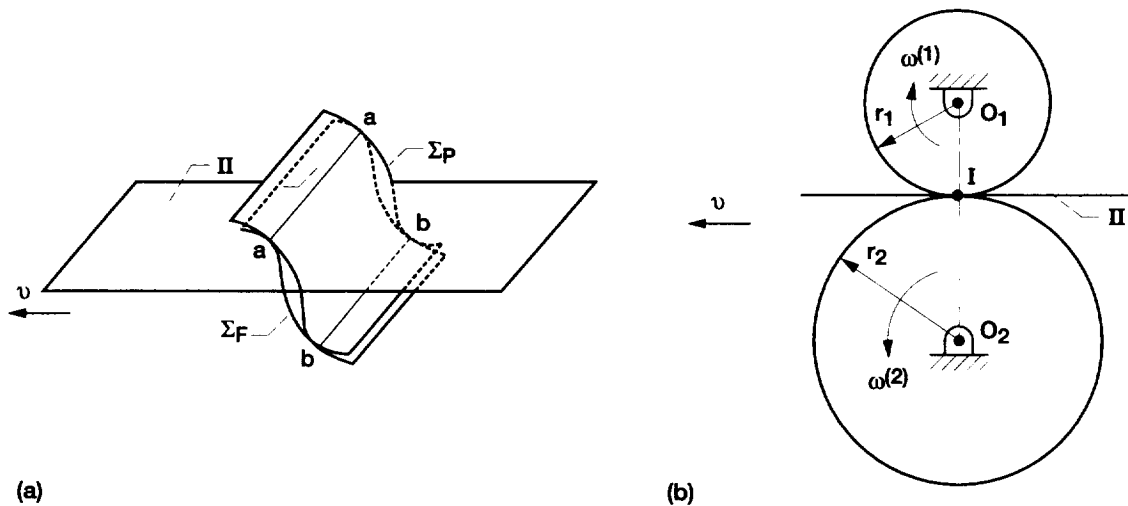


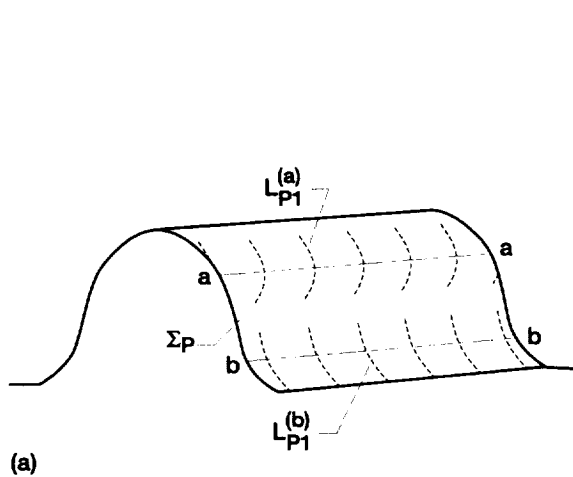
Figure 1.—Axodes and generating surfaces. (a) Rack-cutter surfaces and axode plane. (b) Cross sections of gear axodes.

Figure 2(a) shows two families of contact lines  $L_{P1}^{(a)}$  and  $L_{P1}^{(b)}$  (the upper and the lower ones) on the rack-cutter surface  $\Sigma_P$  that exist when surface  $\Sigma_P$  generates surface  $\Sigma_1$ . Lines  $a - a$  and  $b - b$  are the lines of tangency of rack-cutter surfaces  $\Sigma_P$  and  $\Sigma_F$ . Obviously, contact lines  $L_{P1}^{(a)}$  and  $L_{P1}^{(b)}$  intersect lines  $a - a$  and  $b - b$ , respectively. Similarly, we may represent two families of contact lines  $L_{F2}^{(a)}$  and  $L_{F2}^{(b)}$  on rack-cutter surface  $\Sigma_F$  (fig. 2(b)).

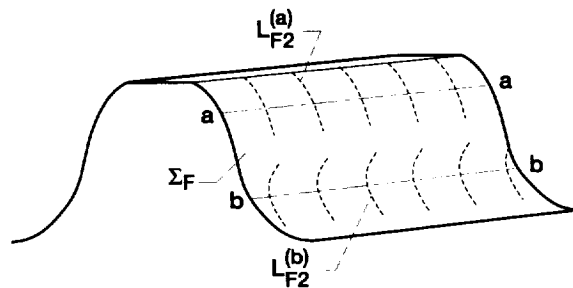
Considering the meshing of generated gear tooth surfaces  $\Sigma_1$  and  $\Sigma_2$ , we recognize immediately that these surfaces are in point contact at every instant. There are two contact points at every instant, the upper and lower points of contact in an ideal gear train. The instantaneous upper point of contact of  $\Sigma_1$  and  $\Sigma_2$ ,  $M^{(a)}$ , is the point of intersection of  $L_{P1}^{(a)}$  with  $a - a$  (fig. 3(a)). The lower instantaneous point of contact of  $\Sigma_1$  and  $\Sigma_2$ ,  $M^{(b)}$ , is the point of intersection of  $L_{P1}^{(b)}$  with  $b - b$ . Obviously,  $M^{(a)}$  may be considered as well as the instantaneous point of intersection of  $L_{F2}^{(a)}$  with  $a - a$  (fig. 3(b));  $M^{(b)}$  is the instantaneous point of intersection of  $L_{F2}^{(b)}$  with  $b - b$ .

The path of contact on surface  $\Sigma_i$  ( $i = 1, 2$ ) is the set of points of  $\Sigma_i$  where  $\Sigma_1$  and  $\Sigma_2$  contact each other. Such a path of contact is a helix, and the contact point moves in the process of meshing along the helix on  $\Sigma_i$  (fig. 3). There are two paths of contact on surface  $\Sigma_i$ , the upper and the lower ones.

The *line of action* is the set of contact points in the fixed coordinate system rigidly connected to the housing of the train. The line of action is a straight line that is parallel to the gear axes. There are two lines of action, the upper and the lower ones.

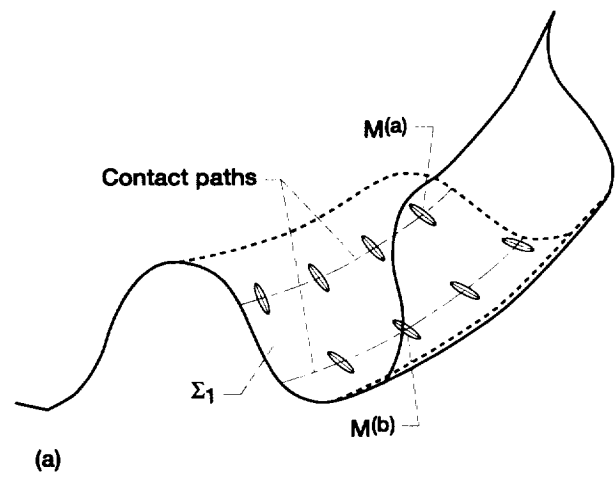


(a)

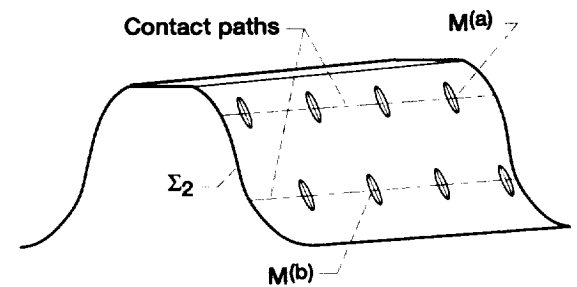


(b)

Figure 2.—Contact lines on generating surface.  
(a) Rack-cutter P. (b) Rack-cutter F.



(a)



(b)

Figure 3.—Paths of contact and contact ellipses on pinion-gear tooth surfaces. (a) On pinion tooth surface. (b) On gear tooth surface.



## 2.1.2 Geometry of Rack-Cutter

### Normal Section of Rack-Cutter

The normal sections of the rack-cutters are represented in figure 4. The profile of the basic tooth of the rack-cutter in the normal section is symmetric about  $y_a$ ; the next tooth can be obtained by the displacement on the circular pitch  $p_n$  of the basic tooth along axis  $x_a$ . Each side of the basic tooth in the normal section consists of three circular arcs. The circular arcs of rack-cutter  $P$  are represented in  $S_a^{(P)}$  by the equations

$$\left. \begin{aligned} x_a^{(P)} &= \rho_P \cos \theta_P + x_{oP} \\ y_a^{(P)} &= \rho_P \sin \theta_P + y_{oP} \\ z_a^{(P)} &= 0 \end{aligned} \right\} \quad (2.1.1)$$

Here,  $\rho_P$  is the radius of circular arc;  $(x_{oP}, y_{oP})$  are the arc center coordinates;  $\theta_P$  is the variable parameter (subscript  $P = a, f, g$ ) (fig. 4). Circular arcs  $a$  and  $f$  generate the working surfaces of the pinion, and  $g$  generates the fillet surface.

The mating rack-cutter  $F$  has the same three circular arcs as those of the rack-cutter  $P$  that can be represented in coordinate system  $S_a^{(F)}$  by using the following equations of coordinate transformation:

$$\left. \begin{aligned} x_a^{(F)} &= -x_a^{(P)} + \frac{p_n}{2} \\ y_a^{(F)} &= -y_a^{(P)} \\ z_a^{(F)} &= 0 \end{aligned} \right\} \quad (2.1.2)$$

where  $p_n = \pi m$ .

The general description in  $S_a^{(t)}$  of all circular arcs for both rack-cutters is as follows:

$$\left. \begin{aligned} x_a^{(t)} &= \rho_t \cos \theta_t + x_{ot} \\ y_a^{(t)} &= \rho_t \sin \theta_t + y_{ot} \\ z_a^{(t)} &= 0 \end{aligned} \right\} \quad (2.1.3)$$

where  $t = F, P$ .

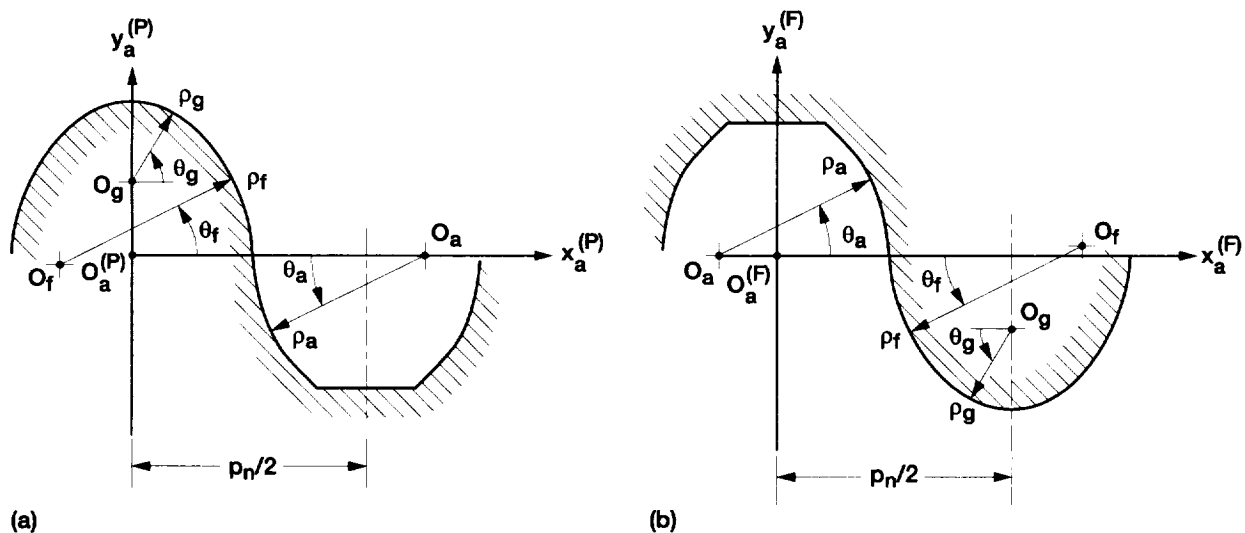


Figure 4.—Derivation of normal section of rack-cutters. (a) Rack-cutter P. (b) Rack-cutter F.

### Tooth Surface of Rack-Cutter

We consider that the normal *section* of the tooth of the rack-cutter is represented in coordinate system  $S_a$  by equations (2.1.3). Our next goal is to represent the *surface* of the rack-cutter tooth in the three-dimensional space defined by coordinate system  $S_t$  (fig. 5). The derivations of such a surface are based on the following considerations:

(1) Coordinate system  $S_a^{(t)}$  with the normal section of the rack-cutter performs a translational motion along the straight line  $\overline{O_t m}$  (fig. 5).

(2) Straight line  $\overline{O_t m}$  is located in plane II that is tangent to the gear axodes and forms angle  $\beta$  with the  $z_t$ -axis that is parallel to the gear axis.

(3) The current location of the origin  $O_a^{(t)}$  in coordinate system  $S_t$  is determined by the variable parameter

$$u_t = \overline{O_t O_a^{(t)}}$$

(4) The surface of the rack-cutter tooth is determined in  $S_t$  by the matrix equation

$$\mathbf{r}_t = \mathbf{M}_{ta} \mathbf{r}_a^{(t)} \quad (2.1.4)$$

where (fig. 5)

$$\mathbf{M}_{ta} = \begin{bmatrix} \cos \beta & 0 & -\sin \beta & -u_t \sin \beta \\ 0 & 1 & 0 & 0 \\ \sin \beta & 0 & \cos \beta & u_t \cos \beta \\ 0 & 0 & 0 & 1 \end{bmatrix} \quad (2.1.5)$$

After derivations we obtain the following equations of the rack-cutter surfaces:

$$\mathbf{r}_t(\theta_t, u_t) = \begin{bmatrix} (\rho_t \cos \theta_t + x_{ot}) \cos \beta - u_t \sin \beta \\ \rho_t \sin \theta_t + y_{ot} \\ (\rho_t \cos \theta_t + x_{ot}) \sin \beta + u_t \cos \beta \end{bmatrix} \quad (2.1.6)$$

where  $t = F, P$  and the surface parameters are  $u_t$  and  $\theta_t$ .

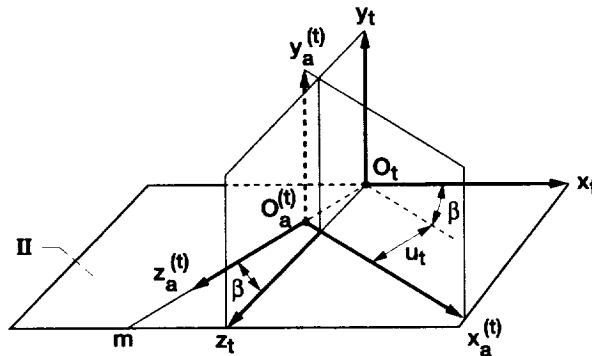


Figure 5.—Derivation of rack-cutter surface.

## Normal to Rack-Cutter Surface

The unit normal to the rack-cutter surface is represented as

$$\mathbf{n}_t = \frac{N_t}{|N_t|}, \quad N_t = \frac{\partial r_t}{\partial \theta_t} \times \frac{\partial r_t}{\partial u_t} \quad (2.1.7)$$

Thus

$$\mathbf{n}_t = \begin{bmatrix} \cos \theta_t \cos \beta \\ \sin \theta_t \\ \cos \theta_t \sin \beta \end{bmatrix} \quad (2.1.8)$$

Equations (2.1.6) and (2.1.8) must be derived four times to represent the upper and lower parts of the working surfaces of two rack-cutters that generate the pinion and the gear, respectively.

### 2.1.3 Equation of Meshing Between Rack-Cutter and Gear Surfaces

#### Applied Coordinate Systems

Movable coordinate systems  $S_t$ ,  $S_1$ , and  $S_2$  are rigidly connected to the tool (the rack-cutter), the pinion, and the gear, respectively. A fixed coordinate system  $S_m$  is rigidly connected to the frame of the cutting machine (fig. 6).

#### Equation of Meshing

The equation of meshing between surface  $\Sigma_t$  ( $t = F, P$ ) of the rack-cutter and the gear tooth surface  $\Sigma_i$  ( $i = 1, 2$ ) must be represented as

$$f(u_t, \theta_t, \phi_i) = 0 \quad (2.1.9)$$

where  $\phi_i$  is the angle of rotation of the gear in the process for generation. The derivation is based on the theorem that the common normal to  $\Sigma_t$  and  $\Sigma_i$  must pass through the instantaneous axis of rotation. Thus, we have

$$\frac{X_t - x_t}{n_{xt}} = \frac{Y_t - y_t}{n_{yt}} = \frac{Z_t - z_t}{n_{zt}} \quad (2.1.10)$$

Here (fig. 6)

$$\left. \begin{array}{l} X_t = s_i = r_i \phi_i \\ Y_t = 0 \\ 0 \leq Z_t \leq l \end{array} \right\} \quad (2.1.11)$$

where  $t = P$  while  $i = 1$ , and  $t = F$  while  $i = 2$ .

Equations (2.1.10), (2.1.11), (2.1.6), and (2.1.8) yield

$$f(u_t, \theta_t, \phi_i) = (r_i \phi_i + u_t \sin \beta - x_{ot} \cos \beta) \sin \theta_t + y_{ot} \cos \theta_t \cos \beta = 0 \quad (2.1.12)$$

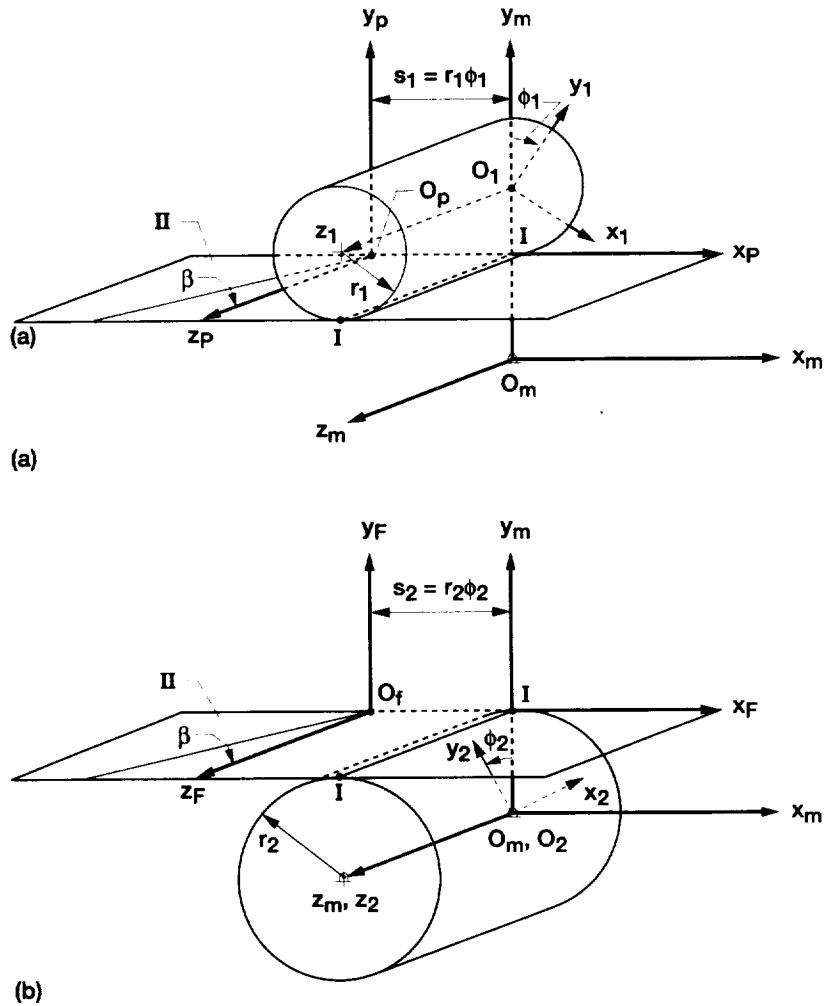


Figure 6.—Derivation of coordinate transformation. (a) For pinion generation. (b) For gear generation.

## 2.2 Geometry of External Gears

### Geometry of Gear Tooth Surface $\Sigma_2$

The generated surface  $\Sigma_2$  (the gear tooth surface) is represented by the family of lines of contact between the rack-cutter surface and the surface of the gear being generated. Analytically, surface  $\Sigma_2$  is represented in  $S_2$  (fig. 6) by the equations

$$r_2(u_F, \theta_F, \phi_2) = M_{2m} M_{mF} r_F, \quad f(u_F, \theta_F, \phi_2) = 0 \quad (2.2.1)$$

Here

$$M_{2m} = \begin{bmatrix} \cos \phi_2 & \sin \phi_2 & 0 & 0 \\ -\sin \phi_2 & \cos \phi_2 & 0 & 0 \\ 0 & 0 & 1 & 0 \\ 0 & 0 & 0 & 1 \end{bmatrix} \quad (2.2.2)$$

$$\mathbf{M}_{mF} = \begin{bmatrix} 1 & 0 & 0 & -r_2\phi_2 \\ 0 & 1 & 0 & r_2 \\ 0 & 0 & 1 & 0 \\ 0 & 0 & 0 & 1 \end{bmatrix} \quad (2.2.3)$$

Equations (2.2.1) represent surface  $\Sigma_2$  in three-parameter form but the parameters are related by the equation of meshing (2.1.12). If we take into account that  $u_F$  is a linear parameter in the equation of meshing, it can be eliminated and surface  $\Sigma_2$  can be represented in two-parameter form, in terms of parameters  $\theta_F$  and  $\phi_2$ . Thus,

$$\left. \begin{aligned} x_2 &= A_2 \sin \phi_2 + B_2 \cos \phi_2 \\ y_2 &= A_2 \cos \phi_2 - B_2 \sin \phi_2 \\ z_2 &= (E_2 - D_2 \phi_2) \tan \beta \end{aligned} \right\} \quad (2.2.4)$$

Here

$$\left. \begin{aligned} A_2 &= \rho_F \sin \theta_F + y_{oF} + r_2 \\ B_2 &= (\rho_F \sin \theta_F + y_{oF} \cot \theta_F) \cos \beta \\ D_2 &= r_2 \cot^2 \beta \\ E_2 &= \rho_F \cos \theta_F \cos \beta + \frac{x_{oF}}{\sin \beta} \cot \beta - y_{oF} \cot \theta_F \cos \beta \cot^2 \beta \end{aligned} \right\} \quad (2.2.5)$$

The unit normal to the gear tooth surface is

$$\mathbf{n}_2(\theta_F, \phi_2) = \mathbf{L}_{2m}(\phi_2) \mathbf{L}_{mF} \mathbf{n}_F(\theta_F) = \begin{bmatrix} \cos \theta_F \cos \beta \cos \phi_2 + \sin \theta_F \sin \phi_2 \\ -\cos \theta_F \cos \beta \sin \phi_2 + \sin \theta_F \cos \phi_2 \\ \cos \theta_F \sin \beta \end{bmatrix} \quad (2.2.6)$$

where

$$\mathbf{L}_{2m}(\phi_2) = \begin{bmatrix} \cos \phi_2 & \sin \phi_2 & 0 \\ -\sin \phi_2 & \cos \phi_2 & 0 \\ 0 & 0 & 1 \end{bmatrix} \quad (2.2.7)$$

$$\mathbf{L}_{mF} = \begin{bmatrix} 1 & 0 & 0 \\ 0 & 1 & 0 \\ 0 & 0 & 1 \end{bmatrix} \quad (2.2.8)$$

and  $\mathbf{n}_F(\theta_F)$  is represented by equation (2.1.8).

### Geometry of Pinion Tooth Surface $\Sigma_1$

Surface  $\Sigma_1$  is generated by rack-cutter tooth surface  $\Sigma_P$  and is represented in  $S_1$  (fig. 6) as follows:

$$r_1(u_P, \theta_P, \phi_1) = M_{1m} M_{mP} r_P, \quad f(u_P, \theta_P, \phi_1) = 0 \quad (2.2.9)$$

Here

$$M_{1m} = \begin{bmatrix} \cos \phi_1 & -\sin \phi_1 & 0 & (r_1 + r_2) \sin \phi_1 \\ \sin \phi_1 & \cos \phi_1 & 0 & -(r_1 + r_2) \cos \phi_1 \\ 0 & 0 & 1 & 0 \\ 0 & 0 & 0 & 1 \end{bmatrix} \quad (2.2.10)$$

$$M_{mP} = \begin{bmatrix} 1 & 0 & 0 & -r_1 \phi_1 \\ 0 & 1 & 0 & r_2 \\ 0 & 0 & 1 & 0 \\ 0 & 0 & 0 & 1 \end{bmatrix} \quad (2.2.11)$$

After elimination of the variable  $u_P$ , we represent  $\Sigma_1$  in terms of  $\theta_P$  and  $\phi_1$  by the following equations:

$$\left. \begin{aligned} x_1 &= -A_1 \sin \phi_1 + B_1 \cos \phi_1 \\ y_1 &= A_1 \cos \phi_1 + B_1 \sin \phi_1 \\ z_1 &= (E_1 - D_1 \phi_1) \tan \beta \end{aligned} \right\} \quad (2.2.12)$$

Here

$$\left. \begin{aligned} A_1 &= \rho_P \sin \theta_P + y_{oP} - r_1 \\ B_1 &= (\rho_P \cos \theta_P + y_{oP} \cot \theta_P) \cos \beta \\ D_1 &= r_1 \cot^2 \beta \\ E_1 &= \rho_P \cos \theta_P \cos \beta + \frac{x_{oP}}{\sin \beta} \cot \beta - y_{oP} \cot \theta_P \cos \beta \cot^2 \beta \end{aligned} \right\} \quad (2.2.13)$$

The unit normal to the pinion tooth surface is

$$\mathbf{n}_2(\theta_P, \phi_1) = L_{1m}(\phi_1) L_{mP} \mathbf{n}_P(\theta_P) = \begin{bmatrix} \cos \theta_P \cos \beta \cos \phi_1 - \sin \theta_P \sin \phi_1 \\ \cos \theta_P \cos \beta \sin \phi_1 + \sin \theta_P \cos \phi_1 \\ \cos \theta_P \sin \beta \end{bmatrix} \quad (2.2.14)$$

where

$$L_{1m}(\phi_1) = \begin{bmatrix} \cos \phi_1 & -\sin \phi_1 & 0 \\ \sin \phi_1 & \cos \phi_1 & 0 \\ 0 & 0 & 1 \end{bmatrix} \quad (2.2.15)$$

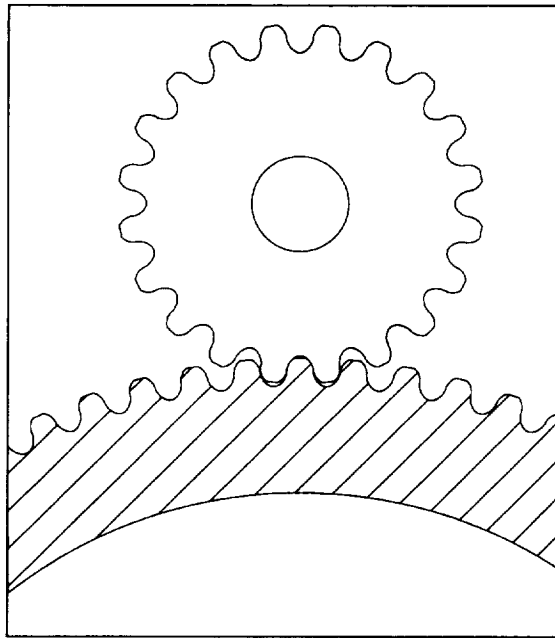


Figure 7.—Transverse section of external gear drive.

$$L_{mP} = \begin{bmatrix} 1 & 0 & 0 \\ 0 & 1 & 0 \\ 0 & 0 & 1 \end{bmatrix} \quad (2.2.16)$$

and  $\mathbf{n}_p(\theta_p)$  is represented by equation (2.1.8).

Figure 7 shows the external gear drive in the transverse section. The gear is a right-hand helical gear, and the pinion is a left-hand helical gear.

### 2.3 Generation of Internal Gears

An internal gear drive of double circular-arc helical gears is composed of an internal gear and an external pinion. The generation of the internal gear tooth surface is based on the following considerations:

(1) The generation of the external gear is performed by an imaginary rack-cutter  $F$  that is shown as figure 8(a). The process of the external gear generation has been mentioned in Section 2.1.

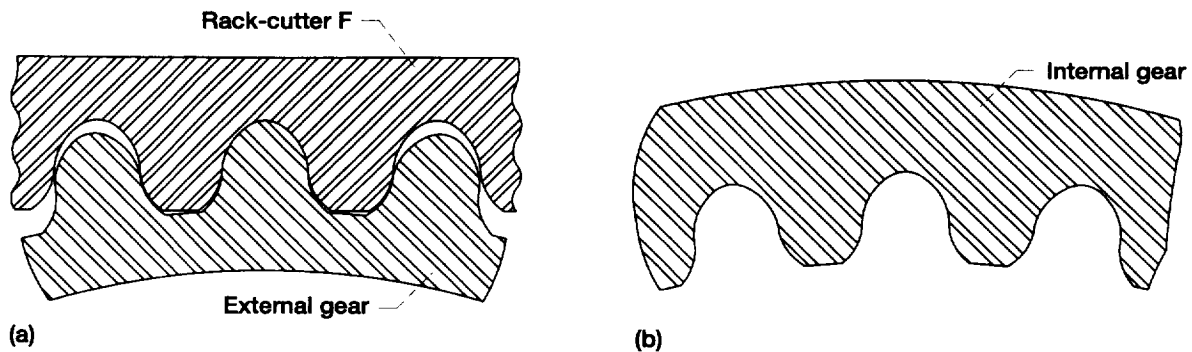


Figure 8.—Double circular-arc internal gear. (a) Generation performed by imaginary rack-cutter  $F$ . (b) Tooth surface of internal gear.

- (2) The gear tooth surface generated by rack-cutter  $F$  is represented by equations (2.2.4) and (2.2.5).
- (3) We consider the gear tooth surface represented by equation (2.2.4) as the tooth surface of an internal gear (fig. 8(b)).
- (4) Such a gear tooth surface of the internal gear can be generated by a disk-cutter  $\Sigma_d$  (see Section 4).

## 2.4 Geometry of Internal Gears

### Imaginary Rack-Cutters

In the derivation of tooth surface equations for an internal gear drive, we still use the imaginary rack-cutters  $\Sigma_t$  ( $t = F, P$ ) represented by equations (2.1.6) and (2.1.8).

### Applied Coordinate Systems

Movable coordinate systems  $S_t, S_1,$  and  $S_2$  are rigidly connected to the tool (the rack-cutter), the pinion, and the gear, respectively. A fixed coordinate system  $S_m$  is rigidly connected to the frame of the cutting machine (fig. 9). The original point  $O_m$  of the coordinate system  $S_m$  coincides with  $O_2$  in the process of derivation of the gear tooth surface and coincides with  $O_1$  in the derivation of the pinion tooth surface.

### Equation of Meshing

The equation of meshing between surface  $\Sigma_t$  ( $t = F, P$ ) of rack-cutter and the internal gear (external pinion) tooth surface  $\Sigma_i$  ( $i = 1, 2$ ) is represented as equation (2.1.12).

### Equations of Gear (Pinion) Tooth Surface

The generated surface  $\Sigma_i$  (the pinion or the gear surface) is represented by the family of lines of contact between the rack-cutter surface and the surface of the pinion (gear) being generated. Both the pinion and the gear are the same hand helical gears since the gear is an internal gear. The tooth surface  $\Sigma_i$  generated by the rack-cutter tooth surface  $\Sigma_t$  can be represented in respective coordinate system  $S_i$  ( $i = 1, 2$ ) by the following equations (fig. 9):

$$r_i(u_t, \theta_t, \phi_i) = M_{im} M_{mt} r_t(u_t, \theta_t), \quad f(u_t, \theta_t, \phi_i) = 0 \quad (2.4.1)$$

The unit normal to the tooth surface is represented as follows:

$$n_i(\theta_t, \phi_i) = L_{im} L_{mt} n_t(\theta_t) \quad (2.4.2)$$

Here,  $i = 1$  when  $t = P$ ,  $i = 2$  when  $t = F$ , and

$$M_{im} = \begin{bmatrix} \cos \phi_i & \sin \phi_i & 0 & 0 \\ -\sin \phi_i & \cos \phi_i & 0 & 0 \\ 0 & 0 & 1 & 0 \\ 0 & 0 & 0 & 1 \end{bmatrix} \quad (2.4.3)$$

$$M_{mt} = \begin{bmatrix} 1 & 0 & 0 & -s_i \\ 0 & 1 & 0 & r_i \\ 0 & 0 & 1 & 0 \\ 0 & 0 & 0 & 1 \end{bmatrix} \quad (2.4.4)$$



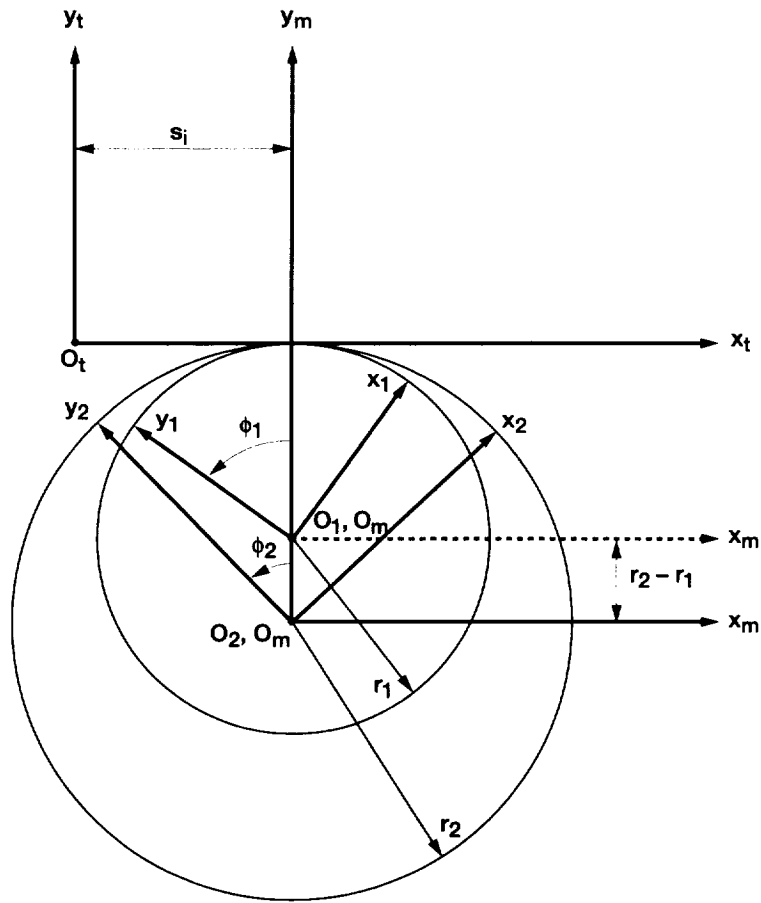


Figure 9.—Derivation of coordinate transformation.

$$L_{im} = \begin{bmatrix} \cos \phi_i & \sin \phi_i & 0 \\ -\sin \phi_i & \cos \phi_i & 0 \\ 0 & 0 & 1 \end{bmatrix} \quad (2.4.5)$$

$$L_{mt} = \begin{bmatrix} 1 & 0 & 0 \\ 0 & 1 & 0 \\ 0 & 0 & 1 \end{bmatrix} \quad (2.4.6)$$

Equations (2.4.1) represent surface  $\Sigma_i$  in three-parameter form but the parameters are related by the equation of meshing. If it is taken into account that  $u_i$  is a linear parameter in the equation of meshing, it can be eliminated and surface  $\Sigma_i$  can be represented in two-parameter form by parameters  $\theta_i, \phi_i$ . Equations (2.4.1), (2.4.3), (2.4.4), (2.1.6), and (2.1.12) yield

$$\left. \begin{aligned} x_i &= A_i \sin \phi_i + B_i \cos \phi_i \\ y_i &= A_i \cos \phi_i - B_i \sin \phi_i \\ z_i &= (E_i - D_i \phi_i) \tan \beta \end{aligned} \right\} \quad (2.4.7)$$

Here

$$\left. \begin{aligned} A_i &= \rho_t \sin \theta_t + y_{ot} + r_i \\ B_i &= (\rho_t \cos \theta_t + y_{ot} \cot \theta_t) \cos \beta \\ D_i &= r_i \cot^2 \beta \\ E_i &= \rho_t \cos \theta_t \cos \beta + \frac{x_{ot} \cot \beta}{\sin \beta} - y_{ot} \cot \theta_t \cos \beta \cot^2 \beta \end{aligned} \right\} \quad (2.4.8)$$

Equations (2.4.2), (2.4.5), (2.4.6), and (2.1.8) yield

$$n_i(\theta_t, \phi_i) = \begin{bmatrix} \cos \theta_t \cos \beta \cos \phi_i + \sin \theta_t \sin \phi_i \\ -\cos \theta_t \cos \beta \sin \phi_i + \sin \theta_t \cos \phi_i \\ \cos \theta_t \sin \beta \end{bmatrix} \quad (2.4.9)$$

Figure 10 shows the internal gear drive in the transverse section.

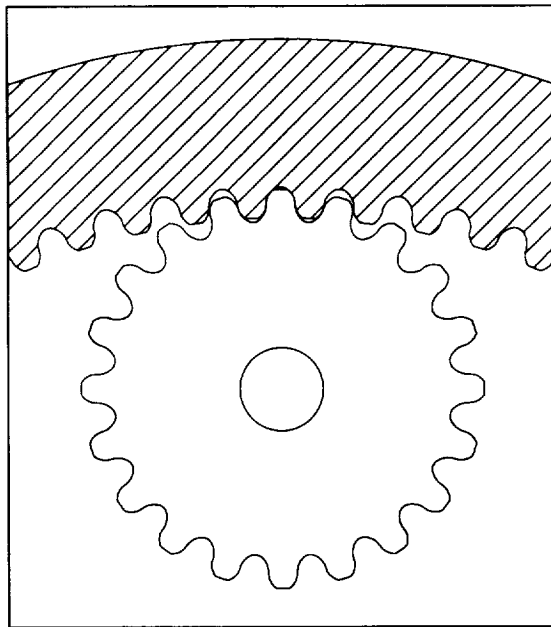


Figure 10.—Transverse section of internal gear drive.

# Chapter 3

## Computerized Simulation of Meshing for Double Circular-Arc Helical Gears

### 3.1 Computerized Simulation of Meshing and Contact

Computerized simulation of meshing is applied to discover the influence of misalignment on the shift of the bearing contact and transmission errors. The misalignment of the gear drive is simulated by the errors of installation and orientation of gear 2 with respect to pinion 1.

#### Applied Coordinate Systems

Coordinate systems  $S_1$ ,  $S_2$ , and  $S_f$  are rigidly connected to the pinion, the gear, and the frame of the gear drive, respectively. To simulate the misalignment of the gear drive, we use auxiliary coordinate systems  $S_p$  and  $S_q$ . The location of  $S_p$  and  $S_q$  with respect to  $S_f$  is shown in figure 11.

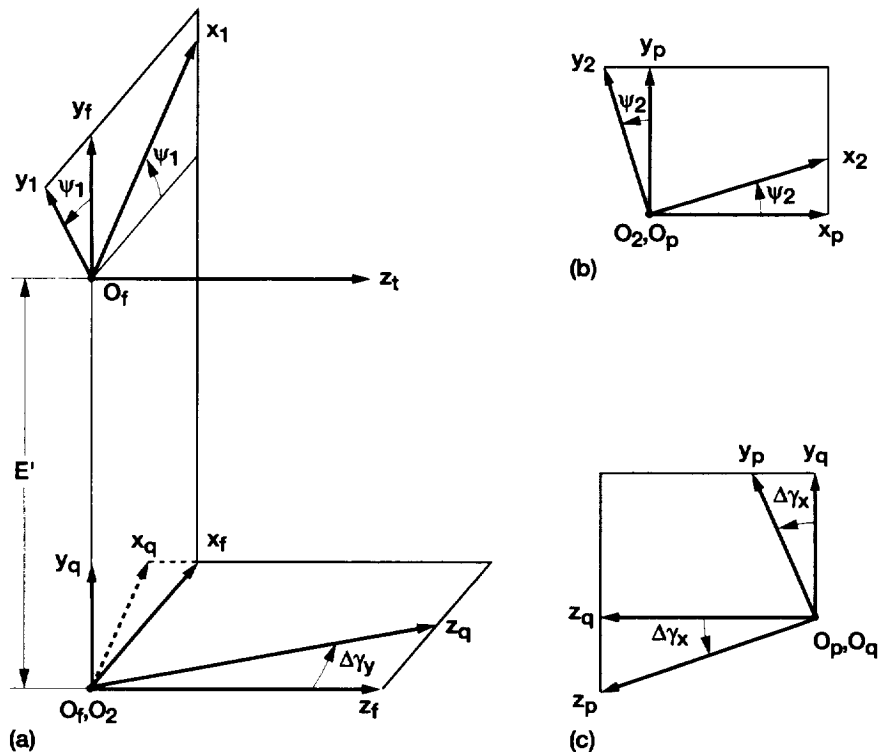


Figure 11.—Coordinate systems applied for simulation of meshing. (a) Installment of coordinate systems  $S_f$ ,  $S_1$ , and  $S_2$ . (b) Installment of coordinate systems  $S_2$  and  $S_p$ . (c) Installment of coordinate systems  $S_p$  and  $S_q$ .

### Conditions of Continuous Tangency

We represent initially the tooth surfaces and the surface unit normals in the fixed coordinate system  $S_f$  by the following equations:

$$\mathbf{r}_f^{(1)} = \mathbf{M}_{f1} \mathbf{r}_1(\theta_P, \phi_1) \quad (3.1.1)$$

$$\mathbf{n}_f^{(1)} = \mathbf{L}_{f1} \mathbf{n}_1(\theta_P, \phi_1) \quad (3.1.2)$$

$$\mathbf{r}_f^{(2)} = \mathbf{M}_{fq} \mathbf{M}_{qp} \mathbf{M}_{p2} \mathbf{r}_2(\theta_F, \phi_2) \quad (3.1.3)$$

$$\mathbf{n}_f^{(2)} = \mathbf{L}_{fq} \mathbf{L}_{qp} \mathbf{L}_{p2} \mathbf{n}_2(\theta_F, \phi_2) \quad (3.1.4)$$

where

$$\mathbf{M}_{f1} = \begin{bmatrix} \cos \psi_i & \pm \sin \psi_i & 0 & 0 \\ \mp \sin \psi_i & \cos \psi_i & 0 & E' \\ 0 & 0 & 1 & 0 \\ 0 & 0 & 0 & 1 \end{bmatrix} \quad (3.1.5)$$

Here

$$E' = \begin{cases} r_2 + r_1 + \Delta E, & \text{for external gear drive} \\ r_2 - r_1 + \Delta E, & \text{for internal gear drive} \end{cases}$$

The upper sign in matrix (3.1.5) is for the external gear drive, and the lower sign is for the internal gear drive.

$$\mathbf{L}_{f1} = \begin{bmatrix} \cos \psi_1 & \pm \sin \psi_1 & 0 \\ \mp \sin \psi_1 & \cos \psi_1 & 0 \\ 0 & 0 & 1 \end{bmatrix} \quad (3.1.6)$$

$$\mathbf{M}_{p2} = \begin{bmatrix} \cos \psi_2 & -\sin \psi_2 & 0 & 0 \\ \sin \psi_2 & \cos \psi_2 & 0 & 0 \\ 0 & 0 & 1 & 0 \\ 0 & 0 & 0 & 1 \end{bmatrix} \quad (3.1.7)$$

$$\mathbf{M}_{qp} = \begin{bmatrix} 1 & 0 & 0 & 0 \\ 0 & \cos \Delta \gamma_x & -\sin \Delta \gamma_x & 0 \\ 0 & \sin \Delta \gamma_x & \cos \Delta \gamma_x & 0 \\ 0 & 0 & 0 & 1 \end{bmatrix} \quad (3.1.8)$$

$$\mathbf{M}_{fq} = \begin{bmatrix} \cos \Delta\gamma_y & 0 & -\sin \Delta\gamma_y & 0 \\ 0 & 1 & 0 & 0 \\ \sin \Delta\gamma_y & 0 & \cos \Delta\gamma_y & 0 \\ 0 & 0 & 0 & 1 \end{bmatrix} \quad (3.1.9)$$

$$\mathbf{L}_{p2} = \begin{bmatrix} \cos \psi_2 & -\sin \psi_2 & 0 \\ \sin \psi_2 & \cos \psi_2 & 0 \\ 0 & 0 & 1 \end{bmatrix} \quad (3.1.10)$$

$$\mathbf{L}_{qp} = \begin{bmatrix} 1 & 0 & 0 \\ 0 & \cos \Delta\gamma_x & -\sin \Delta\gamma_x \\ 0 & \sin \Delta\gamma_x & \cos \Delta\gamma_x \end{bmatrix} \quad (3.1.11)$$

$$\mathbf{L}_{fq} = \begin{bmatrix} \cos \Delta\gamma_y & 0 & -\sin \Delta\gamma_y \\ 0 & 1 & 0 \\ \sin \Delta\gamma_y & 0 & \cos \Delta\gamma_y \end{bmatrix} \quad (3.1.12)$$

The gear tooth surfaces are in continuous tangency that is described by the following equations:

$$\mathbf{r}_f^{(1)} = (\theta_P, \phi_1, \psi_1) = \mathbf{r}_f^{(2)} = (\theta_F, \phi_2, \psi_2) \quad (3.1.13)$$

$$\mathbf{n}_f^{(1)} = (\theta_P, \phi_1, \psi_1) = \mathbf{n}_f^{(2)} = (\theta_F, \phi_2, \psi_2) \quad (3.1.14)$$

Here  $\mathbf{r}_f^{(i)}(\theta, \phi, \psi_i)$  is the position vector of the gear tooth surface in coordinate system  $S_f$ ;  $\mathbf{n}_f^{(i)}(\theta, \phi, \psi_i)$  is the unit normal to the surface.

### Simulation of Meshing

Equations (3.1.13) and (3.1.14) provide a system of five independent equations in six unknowns; that is,

$$f_i = (\theta_P, \phi_1, \psi_1, \theta_F, \phi_2, \psi_2) = 0, \quad (i = 1, 2, \dots, 5) \quad (3.1.15)$$

The surfaces are in point contact, and it is supposed that the respective Jacobian differs from zero. Thus,

$$\frac{D(f_1, f_2, f_3, f_4, f_5)}{D(\theta_P, \phi_1, \theta_F, \phi_2, \psi_2)} \neq 0$$

by assuming that  $\psi_1$  is the input parameter.

The solution of equation system (3.1.15) by the functions

$$\theta_P(\psi_1), \quad \phi_1(\psi_1), \quad \theta_F(\psi_1), \quad \phi_2(\psi_1), \quad \psi_2(\psi_1)$$

enables us to determine the real contact paths (the shift of the bearing contact) and the transmission errors

$$\Delta\psi_2(\psi_1) = \psi_2(\psi_1) - \frac{N_1}{N_2} \psi_1 \quad (3.1.16)$$

Function  $\Delta\psi_2(\psi_1)$  represents the errors of angular positions of gear 2. Function  $\Delta\psi_2(\psi_1) - \Delta\psi_2(0)$  represents the function of transmission errors;  $\Delta\psi_2(0) = \Delta\psi_2(\psi_1)|_{\psi_1=0}$  is the position error of gear 2 at  $\psi_1 = 0$ . The position error  $\Delta\psi_2(0)$  is the angle of so-called compensating turn of gear 2 that enables us to restore the tangency of surfaces at the initial position when  $\psi_1 = 0$ . Because of misalignment, the gear tooth surfaces at the initial angular positions when  $\psi_1 = \psi_2 = 0$  intersect each other or there is a backlash between the surfaces.

### 3.2 Numerical Examples

#### 3.2.1 Example 1 (External Gear Drive)

The numerical computation has been performed for an external gear drive with the following design parameters:  $N_1 = 12$ ,  $N_2 = 94$ ,  $\alpha_n = 27^\circ$ ,  $P_n = 10 \text{ in.}^{-1}$ ,  $\beta = 30^\circ$ .

#### Tooth Contact Analysis for Aligned Gear Drives

Contact paths on the surfaces of a single tooth are shown in figure 12. The investigation shows that two contact points on the surface of a single tooth exist only in a small area of meshing. Two contact points of this kind are shown as the dark ones on the paths of contact. However, if the contact ratio is two, there are two or even more than two instantaneous contact points but they are located on the surfaces of two teeth. The ideal contact paths are helices and called *mean lines*.

#### Change $\Delta E$ of Center Distance

Consider that the center distance is changed from  $E = r_1 + r_2$  to  $E' = r_1 + r_2 + \Delta E$ . Since the gear axes are still parallel, the conditions of meshing are the same as those shown in figure 12. Two instantaneous contact points on a pair of tooth surfaces exist only in a small area of meshing. But the contact paths are shifted up or down from the mean line and are still helices. The errors of angular position of gear 2 are the following: (1)  $\psi_2(0) = 29.43 \text{ arcsec}$  when  $\Delta E = -0.03 \text{ mm}$ ; (2)  $\psi_2(0) = -23.65 \text{ arcsec}$  when  $\Delta E = 0.03 \text{ mm}$ . The transmission errors are equal to zero.

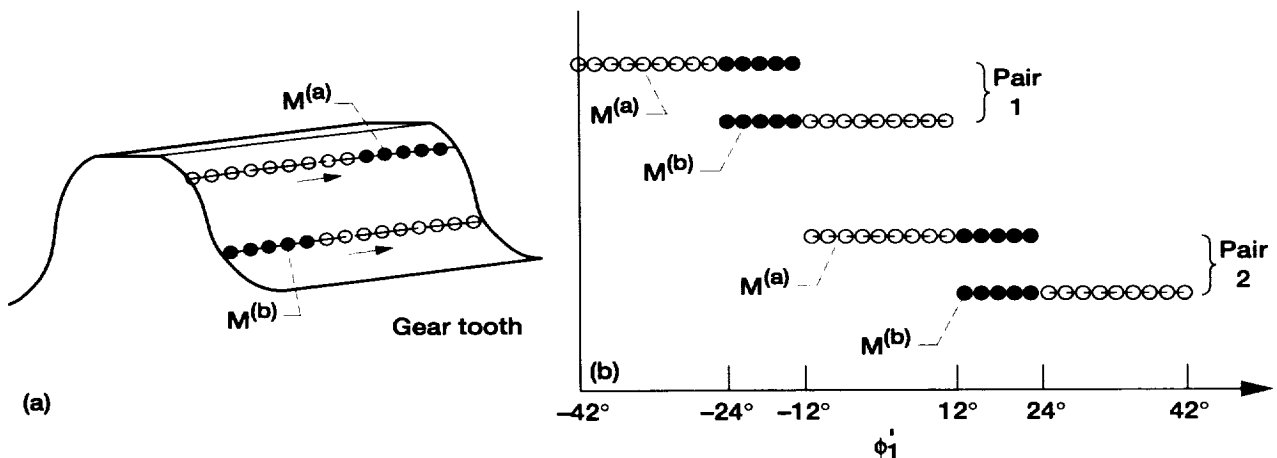


Figure 12.—Sequence of contact points for aligned gear drive. (a) On gear tooth. (b) For meshing of two pairs of teeth.

### Influence of Misalignment $\Delta\gamma_y$ of Gear Axes

The gear axes of an ideal gear train are parallel and might be crossed in a misaligned gear train. The investigation of the influence of crossing angle  $\Delta\gamma_y = \pm 3$  min shows

(1) There is only one instantaneous contact point of gear tooth surfaces  $\Sigma_1$  and  $\Sigma_2$  if the gear axes are crossed: (i) point  $M^{(a)}$  if  $\Delta\gamma_y$  is positive, and (ii) point  $M^{(b)}$  if  $\Delta\gamma_y$  is negative. Surfaces  $\Sigma_1$  and  $\Sigma_2$  are separated at the other theoretical contact point. The backlash between  $\Sigma_1$  and  $\Sigma_2$  measured along the normal is determined as

$$\delta = (r_f^{(1)} - r_f^{(2)}) \cdot n_f \quad (3.2.1)$$

The magnitude of  $\delta$  is 0.008 mm for  $|\Delta\gamma_y| = 3$  min. The instantaneous contact of surfaces at two points can be restored because of lapping or wearing of the surfaces under the load.

(2) Function  $\Delta\psi_2(\psi_1)$  of transmission errors is a piecewise almost linear function with the frequency of a cycle of meshing (fig. 13) for the original gear tooth surfaces. This function is interrupted at the transfer point when one pair of teeth is changed for another one. The jump of transmission errors at the transfer point is the source of noise and vibrations. The maximum transmission error is  $\Delta\psi_{2\max} = 20.84$  arcsec when  $\Delta\gamma_y = \pm 3$  min.

(3) Because of the crossing of gear axes, an angular position error  $\Delta\psi_2(0)$  appears. The value of  $\Delta\psi_2(0)$  is 2.55 arcsec when  $\Delta\gamma_y = \pm 3$  min;  $\Delta\phi_2'(0)$  is 12.97 arcsec when  $\Delta\gamma_y = -3$  min.

### Influence of Errors $\Delta\lambda_F$ of Lead Angle

In the case of an ideal gear drive, the directions of skew teeth of the applied rack-cutters are equal and  $\beta_p = \beta_F$ . Consider now that there is an error  $\Delta\lambda_F$  of the installment of the rack-cutter that generates the gear. Then, an error  $\Delta\lambda_F$  of the gear lead angle on the pitch circle will occur. The investigation of the influence of  $\Delta\lambda_F = \pm 3$  min shows the following results:

The instantaneous contact point is  $M^{(b)}$  if  $\Delta\lambda_F$  is positive and  $M^{(a)}$  if  $\Delta\lambda_F$  is negative. The value of  $\Delta\psi_2(0)$  is 12.97 arcsec when  $\Delta\lambda_F = 3$  min;  $\Delta\psi_2(0)$  is 2.55 arcsec when  $\Delta\lambda_F = -3$  min. The maximum transmission error is  $\Delta\psi_{2\max} = 20.84$  arcsec when  $\Delta\lambda_F = \pm 3$  min.

### 3.2.2 Example 2 (Internal Gear Drive)

The same design parameters that were mentioned in Section 3.2.1 are applied for an internal gear drive. By the computerized simulation of meshing and contact, we have found that the computation results of the internal gear drive are very close to those of the external gear drive.

(1) Consider that the center distance is changed from  $E = r_2 - r_1$  to  $E' = r_2 - r_1 + \Delta E$ . The errors of angular position of gear 2 are (i)  $\psi_2(0) = -29.4476$  arcsec when  $\Delta E = 0.03$  mm; (ii)  $\psi_2(0) = 23.6319$  arcsec when  $\Delta E = -0.03$  mm. The transmission errors are equal to zero.

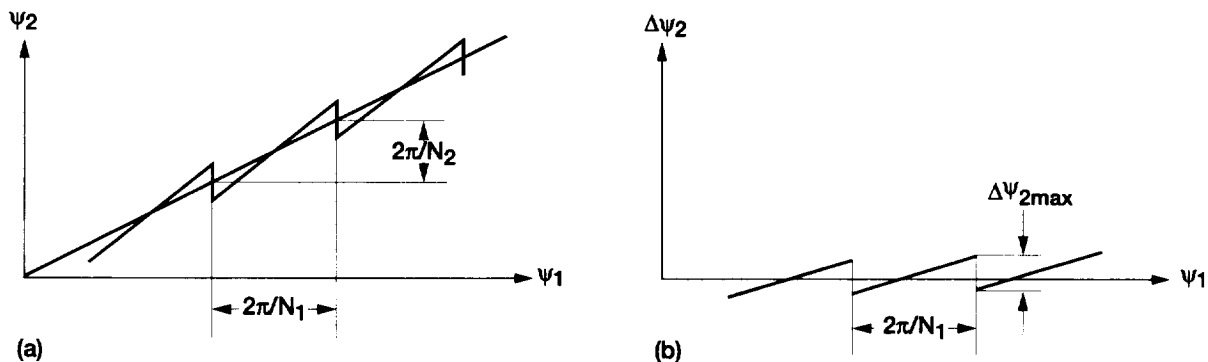


Figure 13.—Transmission function and transmission errors for misaligned gear drive. (a) Transmission function. (b) Transmission errors.

(2) Because of the influence of misalignment error  $\Delta\gamma_y$  of the shaft angle, transmission errors appear as well. The maximum transmission error,  $\Delta\psi_{2\max}$ , is 20.83 arcsec when  $\Delta\gamma_y = 3$  min and 20.85 arcsec when  $\Delta\gamma_y = -3$  min. The value of position error,  $\Delta\psi_2(0)$ , is 2.49 arcsec when  $\Delta\gamma_y = -3$  min;  $\Delta\psi_2(0)$  is 12.94 arcsec when  $\Delta\gamma_y = 3$  min.

(3) In the condition of error  $\Delta\lambda_F$  of lead angle, the angular position errors of gear are  $\Delta\psi_2(0)$  is 12.86 arcsec for  $\Delta\lambda_F = 3$  min; and  $\Delta\psi_2(0) = 2.43$  arcsec for  $\Delta\lambda_F = -3$  min. The maximum transmission error is  $\Delta\psi_{2\max} = 20.84$  arcsec when  $\Delta\lambda_F = \pm 3$  min.

### 3.2. Example 3

The function of transmission errors in one circle of meshing is almost linear when the misalignment of crossing angle  $\Delta\gamma_y$  or error  $\Delta\lambda_F$  of lead angle occurs. The maximum transmission errors for two types of gear drive with the different gear ratios and different helix angle  $\beta$  have been computed numerically, respectively.

#### Case 1: Influence of Gear Ratios

The design parameters are as follows:

$$\beta = 27.6365^\circ, \quad \alpha = 25^\circ, \quad P_n = 5 \frac{1}{\text{in.}}$$

Table I shows the decrease of maximum transmission error  $\Delta\psi_{2\max}$  with the increase of the gear ratio for two types of gear drive for misalignment  $\Delta\gamma_y = 3$  min. Table II shows the maximum transmission error for the lead angle error  $\Delta\lambda_F$ .

#### Case 2: Influence of Helix Angle $\beta$

The design parameters and misalignment are as follows:

$$N_1 = 30, \quad N_2 = 52, \quad \alpha = 25^\circ, \quad P_n = 5 \frac{1}{\text{in.}}, \quad \Delta\gamma_y = 3 \text{ min}$$

Table III shows the decrease of maximum transmission error  $\Delta\psi_{2\max}$  with the increase of the helix angle  $\beta$  for two types of gear drives.

TABLE I.—MAXIMUM TRANSMISSION ERROR WITH CHANGE OF GEAR RATIO ( $\Delta\gamma_y = 3$  min)

Number of teeth of pinion, $N_1$	Number of teeth of gear, $N_2$	External gear drive, arcsec	Internal gear drive, arcsec
30	52	41.56	41.41
30	60	36.02	35.91
20	70	30.87	30.82
20	84	25.72	25.69
12	94	22.98	22.96

TABLE II.—MAXIMUM TRANSMISSION ERROR WITH CHANGE OF GEAR RATIO ( $\Delta\lambda_F = 3$  min)

Number of teeth of pinion, $N_1$	Number of teeth of gear, $N_2$	External gear drive, arcsec	Internal gear drive, arcsec
30	52	41.55	41.55
30	60	36.01	36.01
20	70	30.86	30.86
20	84	25.72	25.72
12	94	22.98	22.98

TABLE III.—MAXIMUM TRANSMISSION ERROR WITH CHANGE OF HELIX ANGLE  $\beta$

Helix angle, $\beta$ , deg	External gear drive, arcsec	Internal gear drive, arcsec
15	81.26	80.77
20	59.81	59.52
25	46.67	46.49
27.6365	41.56	41.41
30	37.69	37.56
35	31.07	30.97
40	25.93	25.85
45	21.75	21.69



# Chapter 4

## Generation of Double Circular-Arc Helical Gears by Grinding Disks

### 4.1 Computerized Design of the Grinding Disks

For an internal gear drive, the grinding disks are designed for the external pinion and internal gear, respectively. For the external gear drive, both of the pinion and gear are external gear tooth surfaces. The approach for the disk design is the same for the cases of external and internal gear drives. Therefore, in this report, the procedure of the design of the grinding disks is presented only for the internal gear drive.

#### Gear Tooth Surfaces

The tooth surface and surface normal of the internal gear (external pinion) have been given by equations (2.4.7) and (2.4.9), respectively. They can be represented by the following equations in two surface parameters ( $u_i, \theta_i$ ):

$$\mathbf{r}_i = \mathbf{r}_i(u_i, \theta_i), \quad (i = 1, 2) \quad (4.1.1)$$

$$\mathbf{n}_i = \mathbf{n}_i(u_i, \theta_i), \quad (i = 1, 2) \quad (4.1.2)$$

#### Equation of Meshing

The derivation of the equation of meshing is based on the following theorem (ref. 5):

*The line of tangency between  $\Sigma_i$  and tool surface  $\Sigma_t$  is such an one at which the normals to  $\Sigma_i$  intersect the rotation axis of the disk-shaped tool.*

The common normal to gear tooth surfaces  $\Sigma_i$  ( $i = 1, 2$ ) and tool surfaces  $\Sigma_t$  ( $t = c, d$ ) is represented by the following equations:

$$\frac{X_i - x_i(u_i, \theta_i)}{n_{xi}(u_i, \theta_i)} = \frac{Y_i - y_i(u_i, \theta_i)}{n_{yi}(u_i, \theta_i)} = \frac{Z_i - z_i(u_i, \theta_i)}{n_{zi}(u_i, \theta_i)} \quad (4.1.3)$$

Here ( $X_t, Y_t, Z_t$ ) are the coordinates in  $S_t$  of the point of intersection of the normal with the  $z_t$ -axis of the tool.

Two grinding disks  $\Sigma_c$  and  $\Sigma_d$  are applied for the external pinion ( $i = 1$ ) and the internal gear ( $i = 2$ ), respectively. The grinding disk  $\Sigma_c$  for the pinion is located above the pitch plane (fig. 14), and the grinding disk  $\Sigma_d$  for gear is located under the pitch plane since the gear is an internal one (the pitch plane is tangent to the pinion-gear pitch cylinders).

We consider the position when  $S_i$  is coincided with  $S_j$  ( $\psi = 0$ ). The point of intersection of the normal with the  $z_t$ -axis can be represented by the equations

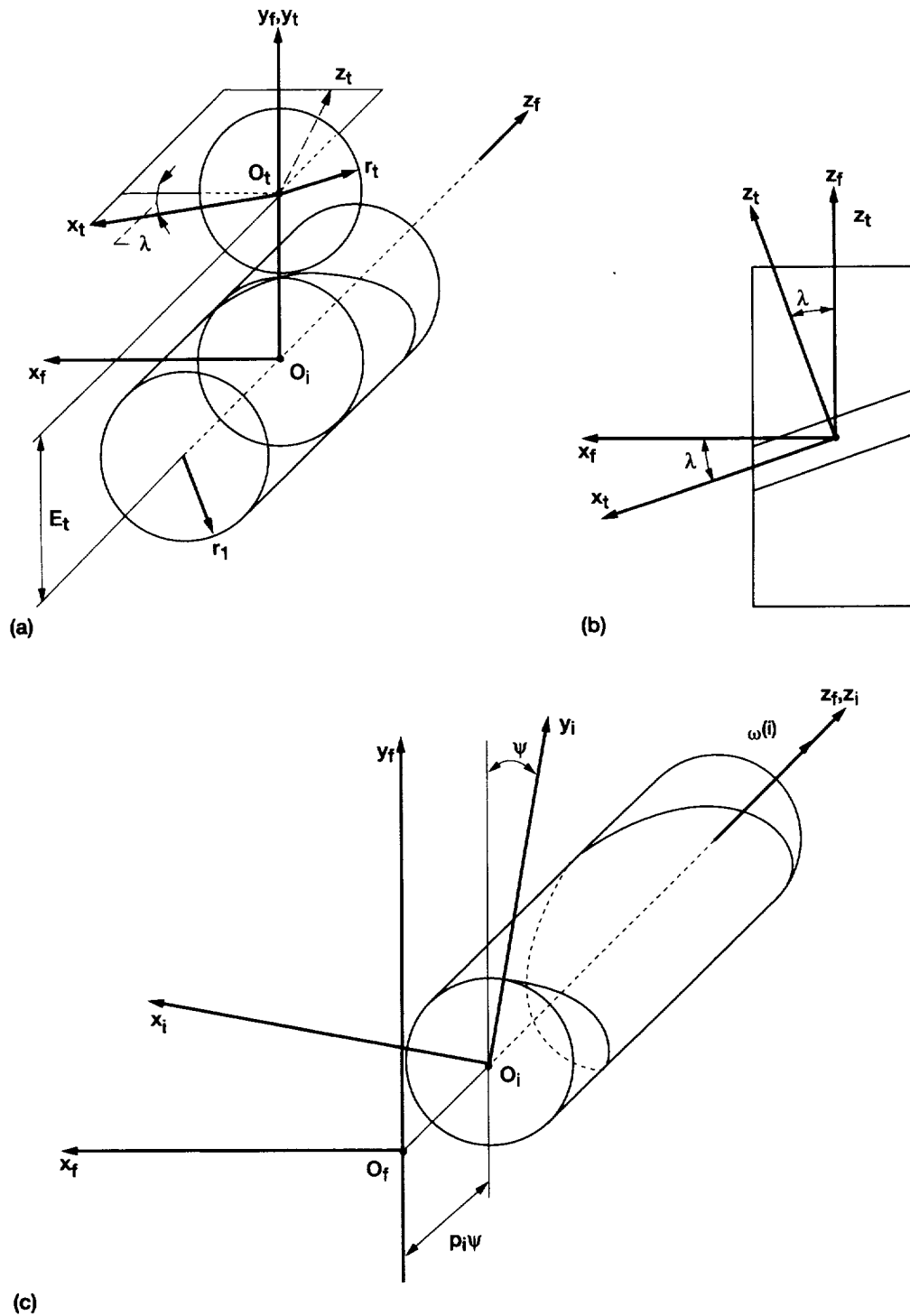


Figure 14.—Coordinate system applied for disk-shape cutter. (a) Installment of coordinate systems  $S_f$  and  $S_t$ . (b) Installment of crossing angle. (c) Illustration of screw motion.

$$\begin{bmatrix} X_i \\ Y_i \\ Z_i \\ 1 \end{bmatrix} = \mathbf{M}_{it} \begin{bmatrix} 0 \\ 0 \\ Z_t \\ 1 \end{bmatrix} = \begin{bmatrix} \cos \lambda & 0 & \sin \lambda & 0 \\ 0 & 1 & 0 & E_t \\ -\sin \lambda & 0 & \cos \lambda & 0 \\ 0 & 0 & 0 & 1 \end{bmatrix} \begin{bmatrix} 0 \\ 0 \\ Z_t \\ 1 \end{bmatrix} \quad (4.1.4)$$

where  $t = c$  while  $i = 1$ ,  $t = d$  while  $i = 2$ ,  $\lambda = 90^\circ - \beta$ , and (fig. 14)

$$E_t = \begin{cases} r_1 + r_{cp}, & \text{(for external pinion when } i = 1) \\ r_2 - r_{dp}, & \text{(for internal gear when } i = 2) \end{cases} \quad (4.1.5)$$

Equations (4.1.3) and (4.1.4) yield

$$\frac{Z_t \sin \lambda - x_i}{n_{xi}} = \frac{E_t - y_i}{n_{yi}} = \frac{Z_t \cos \lambda - z_i}{n_{zi}} \quad (4.1.6)$$

Using equation (4.1.6), we can eliminate  $Z_t$  and simplify the obtained equation of meshing by using the following relation for a helicoid (ref. 5):

$$y_i n_{xi} - x_i n_{yi} - p_i n_{zi} = 0 \quad (4.1.7)$$

Here  $p_i$  is the screw parameter of gear (pinion). The final expression of the equation of meshing is

$$f(u_i, \theta_i) = (E_t - y_i + p_i \cot \lambda) n_{zi} - E_t n_{xi} \cot \lambda + z_i n_{yi} = 0 \quad (4.1.8)$$

### Determination of the Profile of the Grinding Disk

Figure 15 shows the line of tangency of surfaces  $\Sigma_t$  and  $\Sigma_i$  on the cutter surface  $\Sigma_p$ ;  $\mathbf{M}$  is the current point of this line with coordinates  $(x_t, y_t, z_t)$ . The profile of the tool obtained by intersection of plane  $x_t = 0$  (axial section) can be represented by coordinates  $(y_p, z_p)$ . The computational procedure is as follows:

**Step 1:** Use equation of meshing (4.1.8) and consider  $\theta_i$  as the input data; then determine the respective value  $u_i$ .

**Step 2:** Knowing the couple  $(u_i, \theta_i)$ , determine the coordinates  $(x_p, y_p, z_p)$  of the contact line from the matrix equation

$$\mathbf{r}_i(u_i, \theta_i) = \mathbf{M}_{tf} \mathbf{M}_{fi}(\psi = 0) \mathbf{r}_i(u_i, \theta_i) \quad (4.1.9)$$

Here (fig. 14)

$$\mathbf{M}_{fi}(\psi = 0) = \mathbf{I} \quad (4.1.10)$$

$$\mathbf{M}_{tf} \begin{bmatrix} \cos \lambda & 0 & -\sin \lambda & 0 \\ 0 & 1 & 0 & -E_t \\ \sin \lambda & 0 & \cos \lambda & 0 \\ 0 & 0 & 0 & 1 \end{bmatrix} \quad (4.1.11)$$

**Step 3:** Determine  $\rho_i$  using the equation

$$\rho_i(u_i, \theta_i) = (x_i^2 + y_i^2)^{0.5} \quad (4.1.12)$$

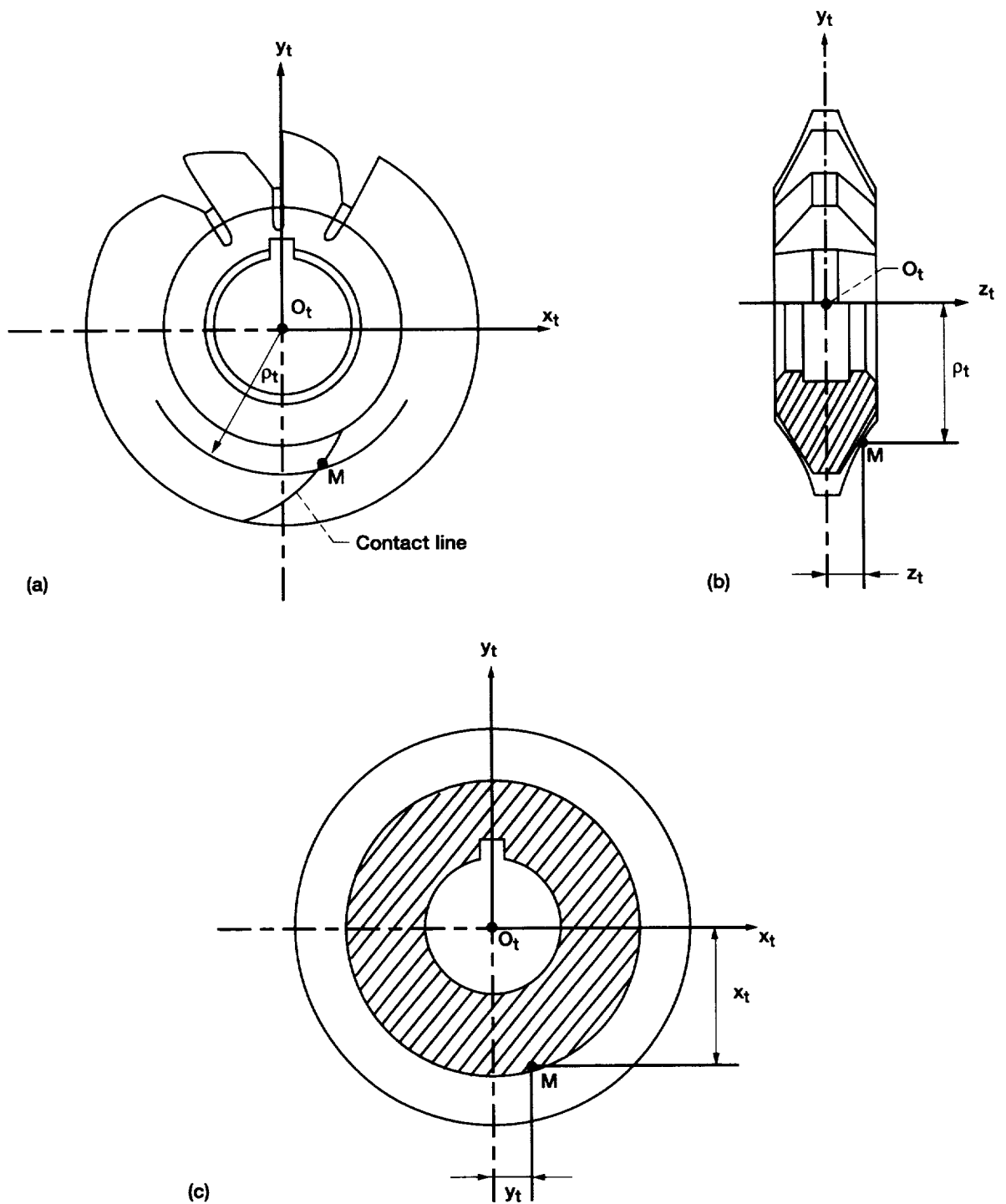


Figure 15.—Derivation of disk-shaped tool profile. (a) Contact line on tool surface. (b) Coordinates  $\rho_t$  and  $z_t$  of contact point. (c) Coordinates  $x_t$  and  $y_t$  of contact point.

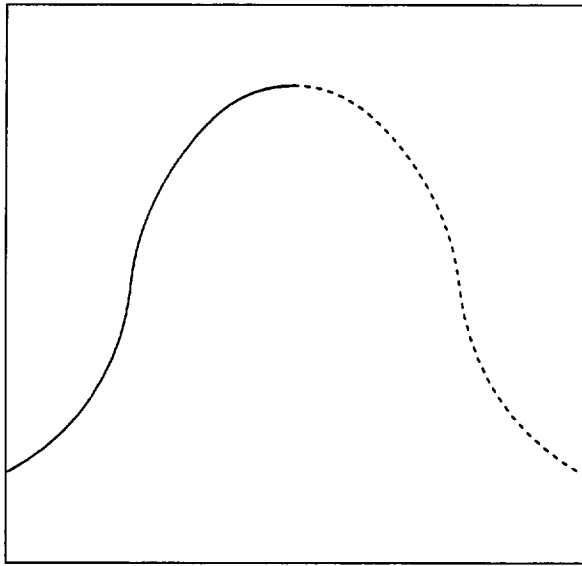


Figure 16.—Axial profile of grinding disk  $\Sigma_C$ .

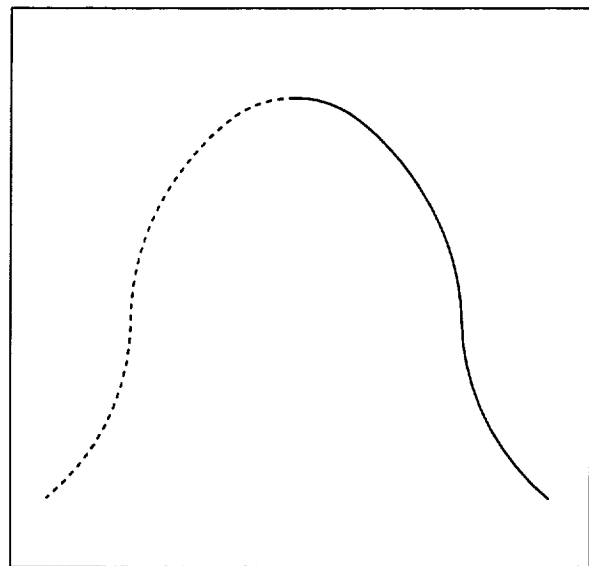


Figure 17.—Axial profile of grinding disk  $\Sigma_D$ .

**Step 4:** Considering  $\theta_i$  as the input parameter and using equations (4.1.9) to (4.1.12), we can determine the tooth profile by the following equations in the axial section of disk:

$$y_t = \rho_t(u_t, \theta_t), \quad z_t = z_t(u_t, \theta_t), \quad f(u_t, \theta_t) = 0 \quad (4.1.13)$$

Figures 16 and 17 show the profiles of grinding disks (axial section) for external pinion and internal gear, respectively.

## 4.2 Generation of Gear (Pinion) Tooth Surface $\Sigma_i$ by Grinding Disk $\Sigma_t$

### Surface of Grinding Disk

The surface of grinding disk  $\Sigma_t$  is a surface of revolution. The axial section is a planar curve  $\alpha - \alpha$  that has been represented in equation (4.1.13). Now it is represented in an auxiliary coordinate system  $S_a$  as follows (fig. 18):

$$x_a = 0, \quad y_a = \rho(u_t), \quad z_a = z(u_t) \quad (4.2.1)$$

where  $u_t$  is the variable parameter that determines the location of a current point of the planar curve  $\alpha - \alpha$ .

The disk surface  $\Sigma_t$  is performed while coordinate system  $S_a$  with the planar curve is rotated about the  $z_t$ -axis (fig. 18). Surface  $\Sigma_t$  is represented in  $S_t$  by the following equation:

$$\mathbf{r}_t(u_t, \theta_t) = \begin{bmatrix} \cos \theta_t & \sin \theta_t & 0 & 0 \\ -\sin \theta_t & \cos \theta_t & 0 & 0 \\ 0 & 0 & 1 & 0 \\ 0 & 0 & 0 & 1 \end{bmatrix} \mathbf{r}_a = \begin{bmatrix} \rho(u_t) \sin \theta_t \\ \rho(u_t) \cos \theta_t \\ z(u_t) \\ 1 \end{bmatrix} \quad (4.2.2)$$

The surface normal is represented in  $S_t$  by the following equation:

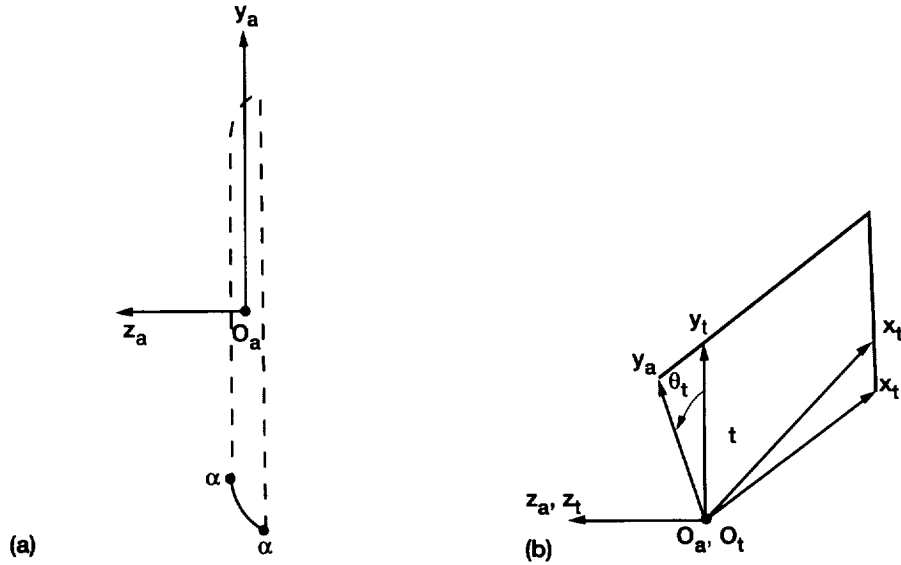


Figure 18.—Disk-shaped tool surface generated by planar curve. (a) Tool axial section. (b) Applied coordinate systems.

$$\mathbf{N}_t = \frac{\partial \mathbf{r}_t}{\partial u_t} \times \frac{\partial \mathbf{r}_t}{\partial \theta_t} = \begin{bmatrix} \rho \frac{\partial z}{\partial u_t} \sin \theta_t \\ \rho \frac{\partial z}{\partial u_t} \cos \theta_t \\ -\rho \frac{\partial \rho}{\partial u_t} \end{bmatrix} \quad (4.2.3)$$

The unit normal to the disk surface is

$$\mathbf{n}_t = \frac{\mathbf{N}_t}{|\mathbf{N}_t|} \quad (4.2.4)$$

### Equation of Meshing

The equation of meshing is represented as

$$\mathbf{n}_t \cdot \mathbf{v}_t^{(ii)} = f(u_t, \theta_t) = 0 \quad (4.2.5)$$

The gear (pinion) performs a screw motion with the angular velocity  $\omega^{(i)}$  and the translational velocity  $p_i \omega^{(i)}$  (fig. 14(c)). The relative velocity  $\mathbf{v}_t^{(ii)}$  is determined by the equation

$$\mathbf{v}_t^{(ii)} = \mathbf{v}_t^{(i)} - \mathbf{v}_t^{(i)} = -\mathbf{v}_t^{(i)} \quad (4.2.6)$$

Since the milling cutter is held at rest, vector  $\mathbf{v}_t^{(i)}$  can be represented by the following equation:

$$\mathbf{v}_t^{(i)} = (\omega_t^{(i)} \times \mathbf{r}_t) + (\mathbf{R}_t \times \omega_t^{(i)}) + p_t \omega_t^{(i)} \quad (4.2.7)$$

Here (fig. 14(a))

$$\mathbf{R}_t = \overline{O_t O_f} = -E_t \mathbf{j}_t \quad (4.2.8)$$

where  $\mathbf{r}_t$  and  $E_t$  are represented by equations (4.2.2) and (4.1.5), respectively. Taking into account that  $\psi = 0$ , we have

$$\omega_t^{(i)} = \mathbf{L}_{tf} \mathbf{L}_{fi}(\psi = 0) \omega_i^{(i)} = \omega^{(i)} \begin{bmatrix} -\sin \lambda \\ 0 \\ \cos \lambda \end{bmatrix} \quad (4.2.9)$$

After transformations, we obtain

$$\mathbf{v}_t^{(i)} = -\omega^{(i)} \begin{bmatrix} -(E_t + y_t) \cos \lambda - p_i \sin \lambda \\ x_t \cos \lambda + z_t \sin \lambda \\ -(E_t + y_t) \sin \lambda + p_i \cos \lambda \end{bmatrix} \quad (4.2.10)$$

There is a relation for a surface of revolution whose axis of rotation is the  $z_t$ -axis

$$x_t n_{yt} - y_t n_{xt} = 0 \quad (4.2.11)$$

The final expression for the equation of meshing is

$$f(u_t, \theta_t) = (E_t \cos \lambda + p_i \sin \lambda) n_{xt} - z_t n_{yt} \sin \lambda + [(E_t + y_t) \sin \lambda - p_i \cos \lambda] n_{zt} = 0 \quad (4.2.12)$$

### Generated Surface

Tooth surface  $\Sigma_i$  is represented in  $S_i$  by the following equations:

$$\mathbf{r}_i(u_t, \theta_t, \psi_i) = \mathbf{M}_{if} \mathbf{M}_{fi} \mathbf{r}_t(u_t, \theta_t), \quad f(u_t, \theta_t) = 0 \quad (4.2.13)$$

where (fig. 14)

$$\mathbf{M}_{if} \begin{bmatrix} \cos \lambda & 0 & \sin \lambda & 0 \\ 0 & 1 & 0 & E_t \\ -\sin \lambda & 0 & \cos \lambda & 0 \\ 0 & 0 & 0 & 1 \end{bmatrix} \quad (4.2.14)$$

$$\mathbf{M}_{if} \begin{bmatrix} \cos \psi_i & \sin \psi_i & 0 & 0 \\ -\sin \psi_i & \cos \psi_i & 0 & 0 \\ 0 & 0 & 1 & -p_i \psi_i \\ 0 & 0 & 0 & 1 \end{bmatrix} \quad (4.2.15)$$

Equations (4.2.13) represent the generated surface in terms of three parameters;  $(u_t, \theta_t, \psi_i)$ , but  $(u_t, \theta_t)$  are related with the equation of meshing (4.2.12).





# Chapter 5

## Generation of Gear Drive With Low Transmission Errors by Application of Imaginary Rack-Cutters

### 5.1 Basic Principle

It was shown in Section 3 that errors of alignment cause a discontinuous almost linear function of transmission errors. The maximal transmission error can reach the value of 40 arcsec that is totally impermissible. Our goals are to change the shape of the function of transmission errors (to obtain it as a parabolic function) and to reduce the level of maximal transmission function. These goals, as it will be shown below, will be achieved if function  $\phi_2(\phi_1)$  is generated as the sum of the theoretical linear function and a predesigned parabolic function. The predesigned parabolic function is able to absorb the almost linear function of transmission errors caused by misalignment. The predesigned parabolic function of transmission errors is obtained because of the modification of the pinion tooth surface or the modification of the gear tooth surface in the case of an external gear drive.

The generation of modified pinion tooth surface is based on application of an imaginary rack-cutter  $\Sigma_p$ . Unlike the case discussed in Section 2, it is necessary to provide the modified relation between the displacement  $s_1$  of rack-cutter  $P$  and angle  $\phi_1$  of pinion rotation (fig. 6 or 9) that is represented as follows:

$$s_1 = r_2 \left( \frac{N_1}{N_2} \phi_1 - a\phi_1^2 \right) \quad (5.1.1)$$

The derivation of equation (5.1.1) is based on the following considerations:

(1) The relation between the displacement  $s_2$  of the rack-cutter  $F$  and angle  $\phi_2$  of gear rotation is still linear and represented as (figs. 6 or 9)

$$s_2 = r_2 \phi_2 \quad (5.1.2)$$

(2) Two imaginary rack-cutters with mismatched surfaces  $\Sigma_t$  ( $t = F, P$ ) are rigidly connected, so we have

$$s_1 = s_2 \quad (5.1.3)$$

(3) The transmission function of the gear drive will be provided as

$$\phi_2 = \frac{N_1}{N_2} \phi_1 - a\phi_1^2 \quad (5.1.4)$$

(4) The predesigned parabolic function will be obtained as

$$\Delta\phi_2 = -a\phi_1^2 \quad (5.1.5)$$

## 5.2 Equation of Meshing

The equation of meshing is represented in coordinate system  $S_i$  of rack-cutter  $P$  as

$$\mathbf{n}_i \bullet \mathbf{v}_i^{(P1)} = f(\theta_P, u_P, \phi_1) = 0 \quad (5.2.1)$$

Here,  $\mathbf{n}_i$  is represented by equation (2.1.8) and the relative velocity,  $\mathbf{v}_i^{(P1)}$ , is derived for external and internal gear drives, respectively.

### Case 1: External Gear Drive

The external pinion in the external gear drive is a left-hand helical gear. The relative velocity between the rack-cutter  $\Sigma_P$  and pinion  $\Sigma_1$  is as follows:

$$\mathbf{v}_P^{(P1)} = \mathbf{v}_P^{(P)} - \mathbf{v}_P^{(1)} \quad (5.2.2)$$

where (fig. 6(a))

$$\mathbf{v}_P^{(P)} = \begin{bmatrix} -\frac{ds_1}{dt} \\ 0 \\ 0 \end{bmatrix} = \begin{bmatrix} -r_2 \left( \frac{N_1}{N_2} - 2a\phi_1 \right) \omega^{(1)} \\ 0 \\ 0 \end{bmatrix} \quad (5.2.3)$$

$$\mathbf{v}_P^{(1)} = \omega_P^{(1)} \times \mathbf{r}_P + \overline{O_P O_1} \times \omega_P^{(1)} \quad (5.2.4)$$

and  $\mathbf{r}_P$  is represented by the equation (2.1.6) and (fig. 6(a))

$$\overline{O_i O_1} = \begin{bmatrix} s_1 \\ r_1 \\ 0 \end{bmatrix}, \quad \omega_i^{(1)} = \begin{bmatrix} 0 \\ 0 \\ -\omega^{(1)} \end{bmatrix} \quad (5.2.5)$$

After transformations, we obtain

$$\mathbf{v}_P^{(P1)} = \omega^{(1)} \begin{bmatrix} -r_2 \left( \frac{N_1}{N_2} - 2a\phi_1 \right) + r_1 - y_P \\ x_P - r_2 \left( \frac{N_1}{N_2} \phi_1 - a\phi_1^2 \right) \\ 0 \end{bmatrix} \quad (5.2.6)$$

The equation of meshing for the left-hand helical pinion is

$$f(u_P, \theta_P, \phi_1) = y_{oP} \cos \theta_P \cos \beta + (r_1 \phi_1 + u_P \sin \beta - x_{oP} \cos \beta) \sin \theta_P - ar_2 (2\phi_1 \cos \theta_P \cos \beta + \phi_1^2 \sin \theta_P) = 0 \quad (5.2.7)$$

### Case 2: Internal Gear Drive

The external pinion in the internal gear drive is a right-hand helical gear. The relative velocity between the rack-cutter  $\Sigma_P$  and pinion  $\Sigma_1$  is as follows:

$$\mathbf{v}_i^{(P1)} = \mathbf{v}_i^{(P)} - \mathbf{v}_i^{(1)} \quad (5.2.8)$$

where (fig. 9)

$$\mathbf{v}_i^{(P)} = \begin{bmatrix} -\frac{ds_1}{dt} \\ 0 \\ 0 \end{bmatrix} = \begin{bmatrix} -r_2 \left( \frac{N_1}{N_2} - 2a\phi_1 \right) \omega^{(1)} \\ 0 \\ 0 \end{bmatrix} \quad (5.2.9)$$

$$\mathbf{v}_i^{(1)} = \omega_i^{(1)} \times \mathbf{r}_P + \overline{O_i O_1} \times \omega_i^{(1)} \quad (5.2.10)$$

and  $\mathbf{r}_P$  is represented by equation (2.1.6) and (fig. 9)

$$\overline{O_i O_1} = \begin{bmatrix} s_1 \\ -r_1 \\ 0 \end{bmatrix}, \quad \omega_i^{(1)} = \begin{bmatrix} 0 \\ 0 \\ \omega^{(1)} \end{bmatrix} \quad (5.2.11)$$

After transformations, we obtain

$$\mathbf{v}_i^{(P1)} = \omega^{(1)} \begin{bmatrix} -r_2 \left( \frac{N_1}{N_2} - 2a\phi_1 \right) + r_1 + y_P \\ -x_P + r_2 \left( \frac{N_1}{N_2} \phi_1 - a\phi_1^2 \right) \\ 0 \end{bmatrix} \quad (5.2.12)$$

The final expression for the equation of meshing is

$$f(u_P, \theta_P, \phi_1) = y_{oP} \cos \theta_P \cos \beta + (r_1 \phi_1 + u_P \sin \beta - x_{oP} \cos \beta) \sin \theta_P + ar_2 (2\phi_1 \cos \theta_P \cos \beta - \phi_1^2 \sin \theta_P) = 0 \quad (5.2.13)$$

### 5.3 Modified Pinion Tooth Surface

The equations of pinion tooth surface are represented in the coordinate system  $S_1$  as

$$\mathbf{r}_1(u_P, \theta_P, \phi_1) = \mathbf{M}_{1m} \mathbf{M}_{mi} \mathbf{r}_i(u_P, \theta_P), \quad f(u_P, \theta_P, \phi_1) = 0 \quad (5.3.1)$$

#### Case 1: External Gear Drive

Matrices in equation (5.3.1) are as follows (fig. 6(a)):

$$\mathbf{M}_{1m} \begin{bmatrix} \cos \phi_1 & -\sin \phi_1 & 0 & 0 \\ \sin \phi_1 & \cos \phi_1 & 0 & 0 \\ 0 & 0 & 1 & 0 \\ 0 & 0 & 0 & 1 \end{bmatrix} \quad (5.3.2)$$

$$\mathbf{M}_{mP} \begin{bmatrix} 1 & 0 & 0 & -s_1 \\ 0 & 1 & 0 & -r_1 \\ 0 & 0 & 1 & 0 \\ 0 & 0 & 0 & 1 \end{bmatrix} \quad (5.3.3)$$

Displacement  $s_1$  in equation (5.3.3) is represented by equation (5.1.1). Equations (2.1.6) and (5.3.1) to (5.3.3) yield

$$\mathbf{r}_1(\theta_P, \phi_1) = \begin{bmatrix} B_1 \cos \phi_1 - A_1 \sin \phi_1 \\ B_1 \sin \phi_1 + A_1 \cos \phi_1 \\ (E_1 - D_1 \phi_1) \tan \beta \end{bmatrix} \quad (5.3.4)$$

where

$$\left. \begin{aligned} A_1(\theta_P) &= \rho_P \sin \theta_P + y_{oP} - r_1 \\ B_1(\theta_P, \phi_1) &= (\rho_P \cos \theta_P + y_{oP} \cot \theta_P - 2a r_2 \phi_1 \cot \theta_P) \cos \beta \\ D_1(\theta_P, \phi_1) &= [r_1 - r_2 a (2 \cot \theta_P \cos \beta + \phi_1)] \cot^2 \beta \\ E_1(\theta_P) &= \rho_P \cos \theta_P \cos \beta + \frac{x_{oP} \cot \beta}{\sin \beta} - y_{oP} \cot \theta_P \cos \beta \cot^2 \beta \end{aligned} \right\} \quad (5.3.5)$$

#### Case 2: Internal Gear Drive

Matrices in equation (5.3.1) are as follows (fig. 9):

$$\mathbf{M}_{1m} \begin{bmatrix} \cos \phi_1 & \sin \phi_1 & 0 & 0 \\ -\sin \phi_1 & \cos \phi_1 & 0 & 0 \\ 0 & 0 & 1 & 0 \\ 0 & 0 & 0 & 1 \end{bmatrix} \quad (5.3.6)$$

$$\mathbf{M}_{mt} = \begin{bmatrix} 1 & 0 & 0 & -s_1 \\ 0 & 1 & 0 & r_1 \\ 0 & 0 & 1 & 0 \\ 0 & 0 & 0 & 1 \end{bmatrix} \quad (5.3.7)$$

The displacement  $s_1$  in equation (5.3.7) is represented by equation (5.1.1). Equations (2.1.6), (5.3.1), (5.3.6), and (5.3.7) yield

$$\mathbf{r}_1(\theta_P, \phi_1) = \begin{bmatrix} A_1 \sin \phi_1 + B_1 \cos \phi_1 \\ A_1 \cos \phi_1 - B_1 \sin \phi_1 \\ (E_1 - D_1 \phi_1) \tan \beta \end{bmatrix} \quad (5.3.8)$$

where

$$\left. \begin{aligned} A_1(\theta_P) &= \rho_P \sin \theta_P + y_{oP} + r_1 \\ B_1(\theta_P, \phi_1) &= (\rho_P \cos \theta_P + y_{oP} \cot \theta_P + 2ar_2 \phi_1 \cot \theta_P) \cos \beta \\ D_1(\theta_P, \phi_1) &= [r_1 + r_2 a (2 \cot \theta_P \cos \beta - \phi_1)] \cot^2 \beta \\ E_1(\theta_P) &= \rho_P \cos \theta_P \cos \beta + \frac{x_{oP} \cot \beta}{\sin \beta} - y_{oP} \cot \theta_P \cos \beta \cot^2 \beta \end{aligned} \right\} \quad (5.3.9)$$

## 5.4 Simulation of Meshing

Equations (3.1.1) to (3.1.16) are applied to determine the bearing contact and the transmission errors. The pinion tooth surface is modified, and the surface vector  $\mathbf{r}_1$  in equation (3.1.1) is represented by equations (5.3.4) and (5.3.5) or equations (5.3.8) and (5.3.9). The gear tooth surface is still a conventional one and can be generated by a grinding disk  $\Sigma_d$  (see Section 4).

The results of computation confirm that the function of transmission errors is indeed a periodic parabolic function and a continuous one (fig. 19). The level of maximal transmission error is substantially reduced (see Tables IV and V).

The numerical results show as well that the influence of errors of alignment is almost the same in external and internal gear drives.

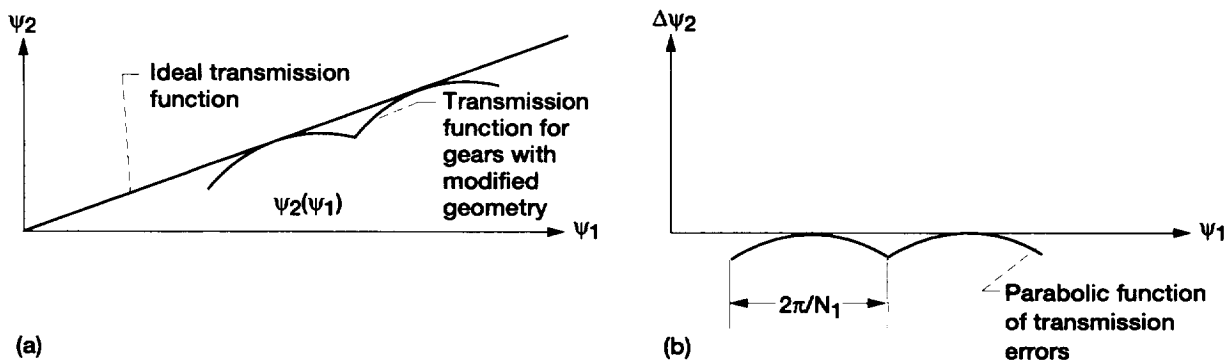


Figure 19.—Transmission function and function of transmission errors for misaligned gear drive. (a) Transmission functions for aligned and misaligned gear drives. (b) Transmission errors.

TABLE IV.—GEAR DRIVE WITH LARGE GEAR RATIO

Number of teeth of pinion, $N_1$ , .....	12
Number of teeth of gear, $N_2$ .....	94
Normal pressure angle, $\alpha_n$ , deg .....	27
Helix angle on the gear (pinion) pitch cylinder, $\beta$ , deg .....	30
Diametral pitch in normal section, $P$ , in <sup>-1</sup> .....	10
Parabola parameter, $\alpha$ .....	0.00053
Crossing angle, $\Delta\gamma$ , min .....	±3
Maximum transmission error, $\Delta\psi_2$ , arcsec .....	8
Tooth length, $L$ , mm .....	37

TABLE V.—GEAR DRIVE WITH SMALL GEAR RATIO

Number of teeth of pinion, $N_1$ , .....	30
Number of teeth of gear, $N_2$ .....	52
Normal pressure angle, $\alpha_n$ , deg .....	25
Helix angle on the gear (pinion) pitch cylinder, $\beta$ , deg .....	27.6365
Diametral pitch in normal section, $P$ , in <sup>-1</sup> .....	5
Parabola parameter, $\alpha$ .....	0.0075
Crossing angle, $\Delta\gamma$ , min .....	±3
Maximum transmission error, $\Delta\psi_2$ , arcsec .....	18
Tooth length, $L$ , mm .....	85

# Chapter 6

## Generation of Modified Pinion by Worms

### 6.1 Introduction

We have determined in Section 5 the modified pinion tooth surface as the envelope to the family of rack-cutter surfaces. Our goal is to prove that the modified pinion tooth surface can be generated as well by a grinding or hobbing worm. The worm thread surface is the envelope to the family of rack-cutter surfaces  $\Sigma_p$ . The worm and pinion being generated perform related rotations about their axes, and the worm performs, in addition, the translational motion in the direction of the axis of the pinion that is called the feed motion. The pinion tooth surface  $\Sigma_1$  generated by a worm can be determined as the envelope to the two-parameter family of worm surfaces, and this can be accomplished by application of the following equations:

$$\mathbf{r}_1 = (u_w, \theta_w, \phi_w, l) = \mathbf{M}_{1w} = (\phi_w, l) \mathbf{r}_w = (u_w, \theta_w) \quad (6.1.1)$$

$$\mathbf{n} \cdot \mathbf{v}^{(w1, \phi_w)} = f_1(u_w, \theta_w, \phi_w, l) = 0 \quad (6.1.2)$$

$$\mathbf{n} \cdot \mathbf{v}^{(w1, l)} = f_2(u_w, \theta_w, \phi_w, l) = 0 \quad (6.1.3)$$

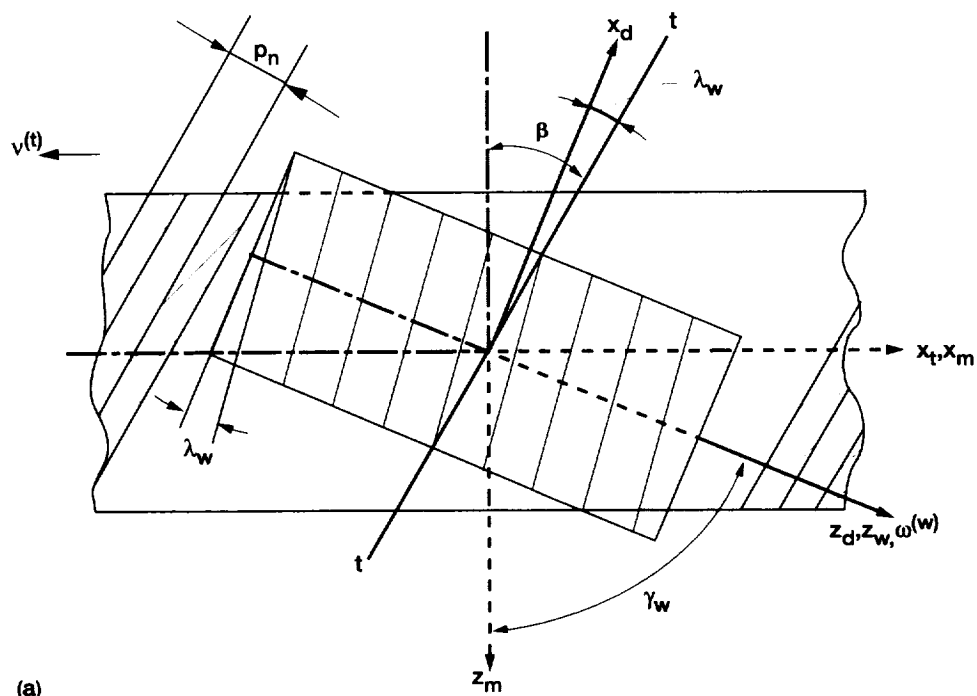
Here,  $(u_w, \theta_w)$  are the surface parameters of worm thread;  $\phi_w$  and  $l$  are the independent parameters of motion in the process for generation;  $\mathbf{v}^{(w1, \phi_w)}$  is the relative velocity determined for the rotational motion of the worm when  $l$  is constant;  $\mathbf{v}^{(w1, l)}$  is the relative velocity determined for the translational motion of the pinion when  $\phi_w$  is constant. The two equations of meshing (6.1.2) and 6.1.3) are required for a two-parameter family of surfaces.

### 6.2 Determination of Worm Thread Surface $\Sigma_w$ Generated by Rack-Cutter Surface $\Sigma_p$

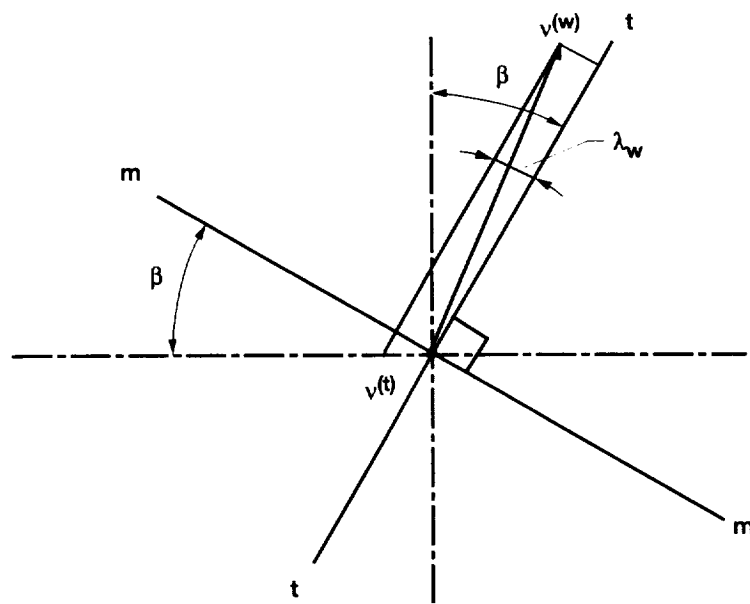
The worm surface  $\Sigma_w$  is determined as the envelope to the family of rack-cutter surfaces  $\Sigma_p$ . Figure 20 shows the installment and the velocity polygon for the case when a right-hand worm is in mesh with the rack-cutter  $P$  generating the right-hand helical pinion. The drawings in figure 20 are represented in plane  $y_t = 0$  that is tangent to the worm pitch cylinder, and the worm is located above the pitch plane. The crossing angle  $\gamma_w$  formed by axis  $z_d$  and  $z_m$  is determined for the discussed case as

$$\gamma_w = 90^\circ - (\beta - \lambda_w) \quad (6.2.1)$$

Figure 21 shows the installment and the velocity polygon for the case when a right-hand worm is in mesh with the rack-cutter  $P$  generating the left-hand helical pinion. The drawings in figure 21 are represented in plane  $y_t = 0$  that is tangent to the worm pitch cylinder, and the worm is located under the pitch plane. The crossing angle  $\gamma_w$  formed by axis  $z_d$  and  $z_m$  is determined for the discussed case as



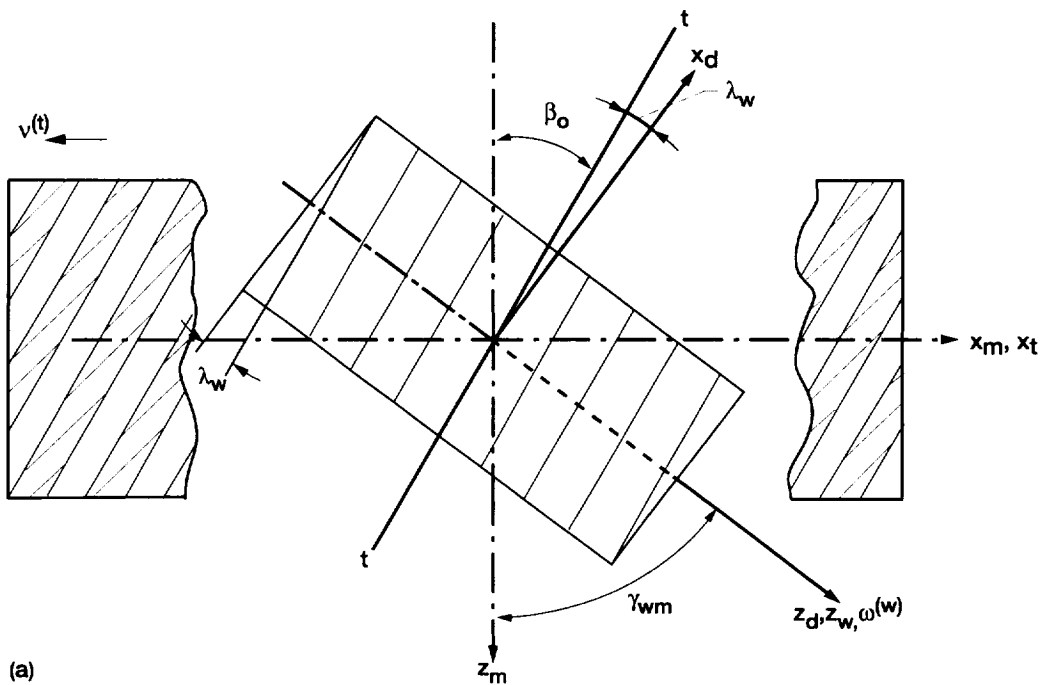
(a)



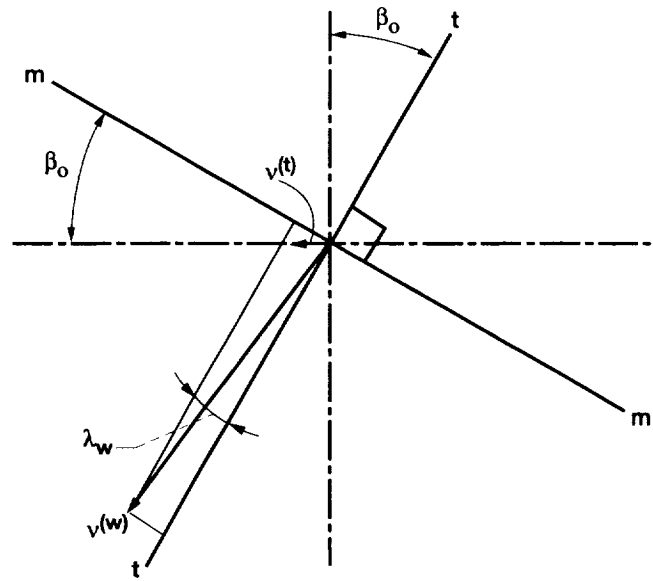
(b)

Figure 20.—Installment of worm, rack-cutter P, and velocity polygon for generation of right-hand pinion. (a) Installment of worm and rack-cutter. (b) Velocity polygon.





(a)



(b)

Figure 21.—Installment of worm, rack-cutter P, and velocity polygon for generation of left-hand pinion. (a) Installment of worm and rack-cutter. (b) Velocity polygon.

$$\gamma_w = 90^\circ - (\beta + \lambda_w) \quad (6.2.2)$$

The derivation of the worm thread surface  $\Sigma_w$  for a right-hand pinion is based on the following considerations:

(1) Movable coordinate systems  $S_w$  and  $S_t$  are rigidly connected to the worm and the rack-cutter  $P$ , respectively; fixed coordinate systems  $S_d$  and  $S_m$  are rigidly connected to the frame of the imaginary generating machine (fig. 22).

(2) The worm and the rack-cutter  $P$  perform rotational and translational motions, respectively (fig. 22). The velocity polygon (fig. 20(b)) provides the following relation between the parameters of motion:

$$\frac{s_1}{\phi_w} = r_{wp} \frac{\sin \lambda_w}{\cos \beta} \quad (6.2.3)$$

(3) The family of rack-cutter surfaces is represented in coordinate system  $S_w$  by the equation

$$\mathbf{r}_w = (u_P, \theta_P, \phi_w) = \mathbf{M}_{wd} \mathbf{M}_{dt} \mathbf{r}_t(u_P, \theta_P) \quad (6.2.4)$$

$$\mathbf{N}^{(w)} \bullet \mathbf{v}^{(wP)} = f(u_P, \theta_P, \phi_w) = 0 \quad (6.2.5)$$

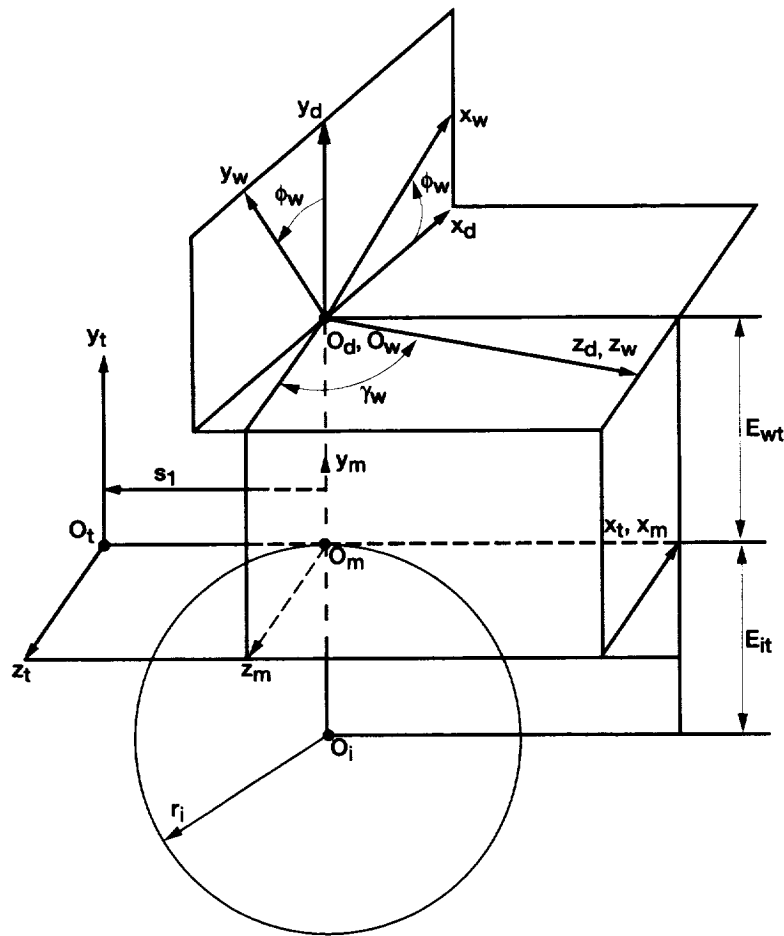


Figure 22.—Derivation of worm thread surface as conjugate to rack-cutter  $P$ .

where (fig. 22)

$$\mathbf{M}_{dt} = \begin{bmatrix} \sin(\beta - \lambda_w) & 0 & -\cos(\beta - \lambda_w) & -s_1 \sin(\beta - \lambda_w) \\ 0 & 1 & 0 & -r_{wp} \\ \cos(\beta - \lambda_w) & 0 & \sin(\beta - \lambda_w) & -s_1 \cos(\beta - \lambda_w) \\ 0 & 0 & 0 & 1 \end{bmatrix} \quad (6.2.6)$$

$$\mathbf{M}_{wd} = \begin{bmatrix} \cos \phi_w & \sin \phi_w & 0 & 0 \\ -\sin \phi_w & \cos \phi_w & 0 & 0 \\ 0 & 0 & 1 & 0 \\ 0 & 0 & 0 & 1 \end{bmatrix} \quad (6.2.7)$$

### Equation of Meshing

The equation of meshing is represented in the coordinate system  $S_m$  as

$$\mathbf{n}_m^{(P)} \bullet \mathbf{v}_m^{(wP)} = f(\theta_P, u_P, \phi_w) = 0 \quad (6.2.8)$$

Here, the unit normal to the rack-cutter surface is represented as

$$\mathbf{n}_m^{(P)} = \mathbf{L}_{mi} \mathbf{n}_i^{(P)} = \mathbf{n}_P(\theta_P) \quad (6.2.9)$$

and the relative velocity is

$$\mathbf{v}_m^{(wP)} = \mathbf{v}_m^{(w)} - \mathbf{v}_m^{(P)} \quad (6.2.10)$$

where  $\mathbf{n}_P$  is represented by equation (2.1.8) and (fig. 22),

$$\mathbf{v}_m^{(P)} = \begin{bmatrix} -\frac{ds_1}{dt} \\ 0 \\ 0 \end{bmatrix} = \begin{bmatrix} -r_{wp} \frac{\sin \lambda_w}{\cos \beta} \omega^{(w)} \\ 0 \\ 0 \end{bmatrix} \quad (6.2.11)$$

$$\mathbf{v}_m^{(w)} = \omega_m^{(w)} \times \mathbf{r}_m^{(w)} + \overline{O_m O_w} \times \omega_m^{(w)} \quad (6.2.12)$$

and

$$\overline{O_m O_w} = \begin{bmatrix} 0 \\ r_{wp} \\ 0 \end{bmatrix}, \quad \omega_m^{(w)} = \omega^{(w)} \begin{bmatrix} \cos(\beta - \lambda_w) \\ 0 \\ \sin(\beta - \lambda_w) \end{bmatrix} \quad (6.2.13)$$

After transformations, we obtain

$$\mathbf{v}_m^{(wP)} = \omega^{(w)} \begin{bmatrix} (r_{wp} - y_p) \sin(\beta - \lambda_w) + r_{wp} \frac{\sin \lambda_w}{\cos \beta} \\ \left( x_p - r_{wp} \frac{\sin \lambda_w}{\cos \beta} \phi_w \right) \sin(\beta - \lambda_w) - z_p \cos(\beta - \lambda_w) \\ -(r_{wp} - y_p) \cos(\beta - \lambda_w) \end{bmatrix} \quad (6.2.14)$$

The final expression for the equation of meshing is

$$f(u_p, \theta_p, \phi_w) = (y_{oP} \cot \theta_p - x_{oP}) \sin \lambda_w - u_p \cos \lambda_w - r_{wp} \frac{\sin \lambda_w}{\cos \beta} \phi_w \sin(\beta - \lambda_w) = 0 \quad (6.2.15)$$

### Worm Thread Surface

The equations of worm thread surface are represented in the coordinate system  $S_w$  as

$$\mathbf{r}_w(u_p, \theta_p, \phi_w) = \mathbf{M}_{wd} \mathbf{M}_{dt} \mathbf{r}_i(u_p, \theta_p), \quad f(u_p, \theta_p, \phi_w) = 0 \quad (6.2.16)$$

The unit normal to the worm thread surface is

$$\mathbf{n}_w(\phi_w, \theta_p) = \mathbf{L}_{wd} \mathbf{L}_{dt} \mathbf{n}_i(\theta_p) \quad (6.2.17)$$

Matrices in equation (6.2.16) are represented by equations (6.2.6) and (6.2.7). Matrices in equation (6.2.17) are represented by the following equations:

$$\mathbf{L}_{dt} = \begin{bmatrix} \sin(\beta - \lambda_w) & 0 & -\cos(\beta - \lambda_w) \\ 0 & 1 & 0 \\ \cos(\beta - \lambda_w) & 0 & \sin(\beta - \lambda_w) \end{bmatrix} \quad (6.2.18)$$

$$\mathbf{L}_{wd} = \begin{bmatrix} \cos \phi_w & \sin \phi_w & 0 \\ -\sin \phi_w & \cos \phi_w & 0 \\ 0 & 0 & 1 \end{bmatrix} \quad (6.2.19)$$

Equations (6.2.16) and (6.2.15) represent the worm thread surface in three-parameter form. Since equation of meshing (6.2.15) is linear with respect to parameters  $u_p$  and  $\phi_w$ , we can eliminate one of them and represent the worm surface by a vector function in terms of two parameters as

$$\mathbf{r}_w = \mathbf{r}_w(u_w, \theta_w) \quad (6.2.20)$$

The worm thread surface generated by rack-cutter surface  $\Sigma_p$  that generates the left- or right-hand helical pinions is exactly the same since the rack-cutters for both cases have the same normal section. The worms that generate the right- and left-hand pinions are located under the pitch plane and above the pitch plane, respectively. It is easy to verify that a worm with the same surface can be used for generation of the right- and left-hand pinions, and this allows us to reduce the tool expenses. The normal section of the worm thread surface differs slightly from the normal section of rack-cutter tooth surface.

### 6.3 Generation of Pinion Tooth Surface by Worm

#### Applied Coordinate Systems

Coordinate systems  $S_w$  and  $S_i$  are rigidly connected to the worm and the right-hand pinion (gear) of internal gear drive, respectively. Fixed coordinate systems  $S_e$  and  $S_n$  are rigidly connected to the cutting (grinding) machine (fig. 23).

#### Relation Between Rotation Angles of Pinion and Worm

The worm and the pinion perform rotational motions. The pinion performs translational motion in the axial direction as the feed motion, and this requires an additional angle of pinion rotation. The axial displacement  $l$  of the pinion can be represented in two components (fig. 24): (1) along the direction of rack-cutter teeth and (2) in the direction that is perpendicular to rotation axis  $z_n$ .

Two cases of derivation of relations between the motion parameters must be considered.

(1) Case 1: The relation between the displacement  $s_i$  of the rack-cutter and angle  $\phi_i$  of the pinion (gear) rotation is linear. Then, the pinion (gear) rotation angle can be represented in two components as

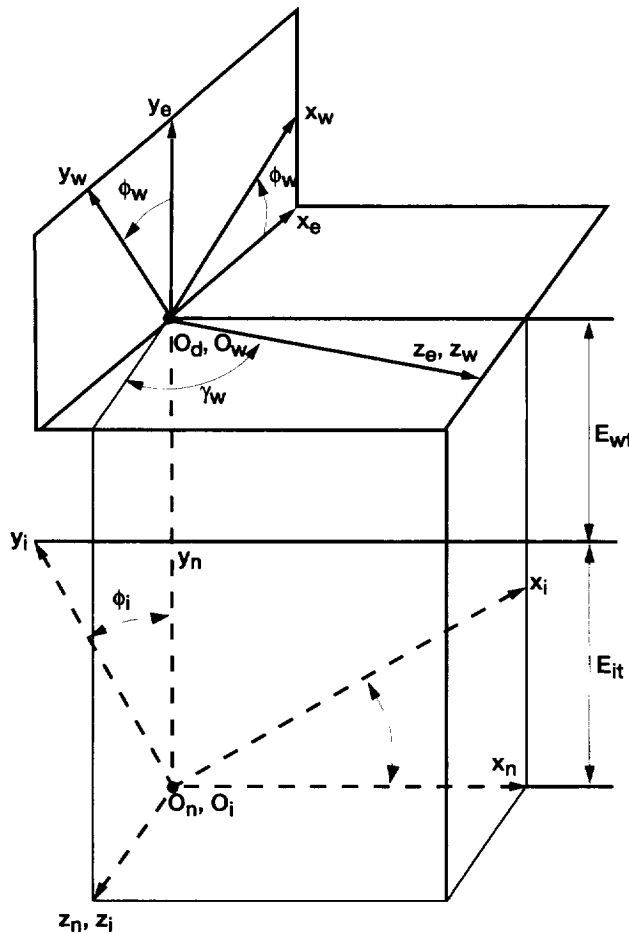


Figure 23.—Coordinate systems applied for generation of right-hand helical gear by worm.

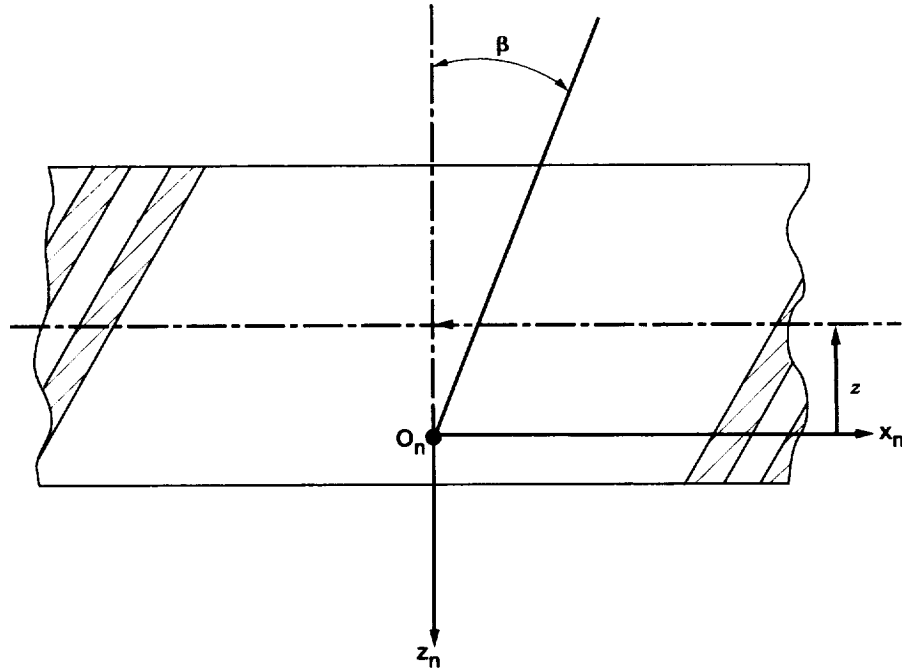


Figure 24.—Determination of relation of motion for generation of helical gear by worm.

$$\phi_i = \frac{s_i}{r_i} - \frac{l \tan \beta}{r_i} = \frac{N_w}{N_i} \left( \phi_w - \frac{l \sin \beta}{r_{wp} \sin \lambda_w} \right) \quad (i = 1, 2) \quad (6.3.1)$$

(2) Case 2: The gear tooth surface is a conventional one, but the pinion tooth surface is modified. Therefore, the relation between parameters of motion of the worm and angle  $\phi_2$  of the gear is represented in two components as

$$\phi_2 = \frac{N_w}{N_2} \left( \phi_w - \frac{l \sin \beta}{r_{wp} \sin \lambda_w} \right) \quad (6.3.2)$$

(3) The transmission function with the predesigned parabolic function of transmission errors must be provided. Thus we have

$$\phi_2 = \frac{N_1}{N_2} \phi_1 - a \phi_1^2 \quad (6.3.3)$$

(4) Equations (6.3.2) and (6.3.3) yield

$$\frac{N_w}{N_2} \left( \phi_w - \frac{l \sin \beta}{r_{wp} \sin \lambda_w} \right) = \left( \frac{N_1}{N_2} \phi_1 - a \phi_1^2 \right) \quad (6.3.4)$$

Equation (6.3.4) represents the relation between the parameters of motion ( $\phi_w, l$ ) and pinion rotation angle  $\phi_1$  when a predesigned parabolic function of transmission errors is provided.

## Pinion Tooth Surface

The pinion tooth surface  $\Sigma_1$  is generated as the envelope to the two-parameter family of worm thread surfaces. The family of rack-cutter surfaces is represented in  $S_1$  as follows:

$$\mathbf{r}_1 = (u_w, \theta_w, \phi_w, l) = \mathbf{M}_{1n}(\phi_1) \mathbf{M}_{ne}(l) \mathbf{M}_{ew}(\phi_w) \mathbf{r}_w(u_w, \theta_w) \quad (6.3.5)$$

$$f_1 = (u_w, \theta_w, \phi_w, l) = \mathbf{n}_1 \bullet \frac{\partial \mathbf{r}_1}{\partial \phi_w} = 0 \quad (6.3.6)$$

$$f_2 = (u_w, \theta_w, \phi_w, l) = \mathbf{n}_1 \bullet \frac{\partial \mathbf{r}_1}{\partial l} = 0 \quad (6.3.7)$$

Here (fig. 23)

$$\mathbf{M}_{ew} = \begin{bmatrix} \cos \phi_w & -\sin \phi_w & 0 & 0 \\ \sin \phi_w & \cos \phi_w & 0 & 0 \\ 0 & 0 & 1 & 0 \\ 0 & 0 & 0 & 1 \end{bmatrix} \quad (6.3.8)$$

$$\mathbf{M}_{ne} = \begin{bmatrix} \sin(\beta - \lambda_w) & 0 & \cos(\beta - \lambda_w) & 0 \\ 0 & 1 & 0 & r_{wp} + r_1 \\ -\cos(\beta - \lambda_w) & 0 & \sin(\beta - \lambda_w) & l \\ 0 & 0 & 0 & 1 \end{bmatrix} \quad (6.3.9)$$

$$\mathbf{M}_{1n} = \begin{bmatrix} \cos \phi_1 & \sin \phi_1 & 0 & 0 \\ -\sin \phi_1 & \cos \phi_1 & 0 & 0 \\ 0 & 0 & 1 & 0 \\ 0 & 0 & 0 & 1 \end{bmatrix} \quad (6.3.10)$$

## Equations of Meshing

Equations 6.3.5) and (6.3.8) to (6.3.10) yield

$$\left. \begin{aligned} x_1 &= D \cos \phi_1 + C \sin \phi_1 \\ y_1 &= -D \sin \phi_1 + C \cos \phi_1 \\ z_1 &= -B \cos(\beta - \lambda_w) + z_w \sin(\beta - \lambda_w) + l \end{aligned} \right\} \quad (6.3.11)$$

where

$$\left. \begin{aligned} A &= x_w \sin \phi_w + y_w \cos \phi_w \\ B &= x_w \cos \phi_w - y_w \sin \phi_w \\ C &= A + r_1 + r_{wp} \\ D &= B \sin(\beta - \lambda_w) + z_w \cos(\beta - \lambda_w) \end{aligned} \right\} \quad (6.3.12)$$

Relative velocities can be obtained by the derivations of equation (6.3.11) and are represented as

$$\mathbf{v}^{(w1,\phi_w)} = \frac{\partial \mathbf{r}_1}{\partial \phi_w} = \begin{bmatrix} (-D \sin \phi_1 + C \cos \phi_1) \frac{\partial \phi_1}{\partial \phi_w} - A \sin(\beta - \lambda_w) \cos \phi_1 + B \sin \phi_1 \\ -(D \cos \phi_1 + C \sin \phi_1) \frac{\partial \phi_1}{\partial \phi_w} + A \sin(\beta - \lambda_w) \sin \phi_1 + B \cos \phi_1 \\ A \cos(\beta - \lambda_w) \end{bmatrix} \quad (6.3.13)$$

$$\mathbf{v}^{(w1,l)} = \frac{\partial \mathbf{r}_1}{\partial l} = \begin{bmatrix} (-D \sin \phi_1 + C \cos \phi_1) \frac{\partial \phi_1}{\partial l} \\ -(D \cos \phi_1 + C \sin \phi_1) \frac{\partial \phi_1}{\partial l} \\ 1 \end{bmatrix} \quad (6.3.14)$$

The partial derivatives,  $\partial \phi_1 / \partial \phi_w$  and  $\partial \phi_1 / \partial l$ , in equations (6.3.13) and (6.3.14) are derived from equation (6.3.4) and are represented as

$$\frac{\partial \phi_1}{\partial \phi_w} = \frac{N_w}{N_1 - 2aN_2\phi_1} \quad (6.3.15)$$

$$\frac{\partial \phi_1}{\partial l} = \frac{N_w \sin \beta}{(N_1 - 2aN_2\phi_1)r_{wp} \sin \lambda_w} \quad (6.3.16)$$

The unit normal to the pinion surface is

$$\mathbf{n}_1 = \mathbf{L}_{1n} \mathbf{L}_{ne} \mathbf{L}_{ew} \mathbf{n}_w(u_w, \theta_w) \quad (6.3.17)$$

where (fig. 23)

$$\mathbf{L}_{ew} = \begin{bmatrix} \cos \phi_w & -\sin \phi_w & 0 \\ \sin \phi_w & \cos \phi_w & 0 \\ 0 & 0 & 1 \end{bmatrix} \quad (6.3.18)$$

$$\mathbf{L}_{ne} = \begin{bmatrix} \sin(\beta - \lambda_w) & 0 & \cos(\beta - \lambda_w) \\ 0 & 1 & 0 \\ -\cos(\beta - \lambda_w) & 0 & \sin(\beta - \lambda_w) \end{bmatrix} \quad (6.3.19)$$

$$\mathbf{L}_{1n} = \begin{bmatrix} \cos \phi_1 & \sin \phi_1 & 0 \\ -\sin \phi_1 & \cos \phi_1 & 0 \\ 0 & 0 & 1 \end{bmatrix} \quad (6.3.20)$$

Equations (6.3.13) to (6.3.20) yield equations of meshing (6.3.6) and (6.3.7).



# Chapter 7

## Directions for Users of Application of Computer Programs

There are four programs described in this report. The programs were developed by application of the IBM Main Frame. The operating system is CMS-9.0.

A subroutine DNEQNF of IMSL software to solve a system of nonlinear equations should be available in the Math-Library or working environment. The subroutine is not included in the programs. Each program will call the subroutine DNEQNF several times.

### 7.1 Program 1: Design of External Gear Drive

#### 7.1.1 Name of the Program

The developed program's name, EGDUIC.FORTRAN, is formed by six characters. The first three characters, EGD, are the initial letters of External Gear Drive. The following three characters, UIC, mean that the program is developed at the University of Illinois at Chicago. The program name is easy to remember before the start of computations.

The extension name of the program is FORTRAN. It means that the program is written in standard FORTRAN77 language.

#### 7.1.2 Function of the Program

This program is developed to design the external helical gear drive of double circular-arc teeth. The program includes (1) generation of helical pinion and gear of double circular-arc teeth by rack-cutters, respectively; (2) tooth contact analysis of contact paths, contact ellipse, and parabolic transmission errors; and (3) generation of external gear drive with low transmission errors by application of imaginary rack-cutters. The equations in the program have been represented in Sections 3 and 5.

#### 7.1.3 Input Data File 90

Before running the program, you should prepare the following data in data file 90:

Helix angle (fig. 5)	$\beta$ (degree)
Diametral pitch	$P_d$ (1/in.)
Number of gear teeth	$N_g$
Number of pinion teeth	$N_p$
Pressure angle (fig. 25)	$\alpha$ (degree)

Error of crossing angle (fig. 11)	$\Delta\gamma_y$ (degree)
Error of center distance	$\Delta C$ (in.)
Error of intersection angle (fig. 11)	$\Delta\gamma_x$ (degree)
Error of gear leader angle	$\Delta\lambda_F$ (degree)
Coefficient of parabolic parameter	$a$

and profile parameters of a rack-cutter in normal section (fig. 25):  $h_a^*$ ,  $c^*$ ,  $\rho_a^*$ ,  $\rho_f^*$ , and  $\Delta e^*$ . Here  $\rho_a = \rho_a^*/P_d$  (or  $\rho_a^*m$ ).

#### 7.1.4 Running the Program

The command for running a program in CMS system is as follows:

```
fortvclg EGDUIIC <Enter>
```

When you run the program, the following information will appear on the screen:

```
*** WELCOME TO USE EGDUIIC ***

END OF READING THE INPUT DATA!

STARTING THE TOOTH CONTACT ANALYSIS!

END OF TCA FOR THE LOWER CONTACT PATH!

END OF TCA FOR THE UPPER CONTACT PATH!

PROGRAM FINISHED!
```

#### 7.1.5 Output Data Files

When you finish running the program, EGDUIIC, you have completed the design for the external helical gear drive of a double circular arc. All information about the output data is listed in several data files. You can open these files and look through them. Detailed information about these output files is given in the following sections:

##### Data File 09:

It includes the input information and pitch radii of gears.

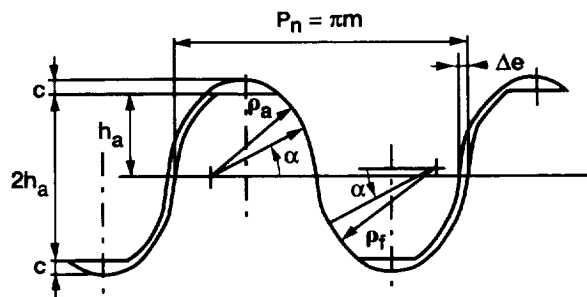


Figure 25.—USSR standard.

**Data File 41:**

This is the lower contact path  $M^{(b)}$  (fig. 3) represented on the pinion tooth surface. Each line of the data file represents coordinates  $(x_1, y_1, z_1)$  of a contact point of the contact path. The coordinates are represented in pinion coordinate system  $S_1$ . The applied unit is mm, and the format is **3F22.14**.

**Data File 42:**

This is the lower contact path  $M^{(b)}$  (fig. 3) represented on the gear tooth surface. Each line of the data file represents coordinates  $(x_2, y_2, z_2)$  of a contact point of the contact path. The coordinates are represented in gear coordinate system  $S_2$ . The applied unit is mm, and the format is **3F22.14**.

**Data File 43:**

This is the upper contact path  $M^{(a)}$  (fig. 3) represented on the pinion tooth surface. Each line of the data file represents coordinates  $(x_1, y_1, z_1)$  of a contact point of the contact path. The coordinates are represented in pinion coordinate system  $S_1$ . The applied unit is mm, and the format is **3F22.14**.

**Data File 44:**

This is the upper contact path  $M^{(a)}$  (fig. 3) represented on the gear tooth surface. Each line of the data file represents coordinates  $(x_2, y_2, z_2)$  of a contact point of the contact path. The coordinates are represented in gear coordinate system  $S_2$ . The applied unit is mm, and the format is **3F22.14**.

**Data File 51:**

There are two curves in this data file for representation of the cross section of a pinion tooth. Each curve is composed of 30 points. Each line of the data file represents coordinates  $(x_1, y_1, z_1)$  of a point of the curve. The coordinates are represented in pinion coordinate system  $S_1$ . The applied unit is mm, and the format is **3F22.14**.

**Data File 52:**

There are two curves in this data file for representation of the cross section of a gear tooth. Each curve is composed of 30 points. Each line of the data file represents coordinates  $(x_2, y_2, z_2)$  of a point of the curve. The coordinates are represented in gear coordinate system  $S_2$ . The applied unit is mm, and the format is **3F22.14**.

**Data File 55:**

It contains transmission errors of one meshing cycle for upper contact path  $M^{(a)}$  (fig. 3). They are obtained by tooth contact analysis (TCA). The format is as follows:

$\phi_{11}$ (degree)	$\Delta\phi_{21}$ (arcsec)
$\phi_{12}$ (degree)	$\Delta\phi_{22}$ (arcsec)
$\phi_{13}$ (degree)	$\Delta\phi_{23}$ (arcsec)
...	...
$\phi_{1i}$ (degree)	$\Delta\phi_{2i}$ (arcsec)
...	...

**Data File 56:**

It contains transmission errors of one meshing cycle for lower contact path  $M^{(b)}$  (fig. 3). The format is the same as that in data file 55.

**Data File 57:**

It contains the values of major and minor axes of upper contact ellipse  $M^{(a)}$  corresponding to the contact points given in data file 43 or 44. The applied unit is mm.

**Data File 58:**

It contains the values of major and minor axes of lower contact ellipse  $M^{(b)}$  corresponding to the contact points given in data file 41 or 42. The applied unit is mm.

**Data File 71:**

This file is designated for drawing of the major axes of contact ellipses,  $M^{(b)}$ , on pinion tooth surface corresponding to the contact points given in data file 41. Each major axis is composed of 3 points. Each line of the data file represents coordinates  $(x_1, y_1, z_1)$  of a point. Each 3-line segment of the data file performs one major axis. The coordinates are represented in pinion coordinate system  $S_1$ . The applied unit is mm, and the format is **3F22.14**.

**Data File 72:**

This file is designated for drawing of the major axes of contact ellipses,  $M^{(b)}$ , on the gear tooth surface corresponding to the contact points given in data file 42. Each major axis is composed of 3 points. Each line of the data file represents coordinates  $(x_2, y_2, z_2)$  of a point. Each 3-line segment of the data file performs one major axis. The coordinates are represented in gear coordinate system  $S_2$ . The applied unit is mm, and the format is **3F22.14**.

**Data File 73:**

This file is designated for drawing of the major axes of contact ellipses,  $M^{(a)}$ , on the pinion tooth surface corresponding to the contact points given in data file 41. Each major axis is composed of 3 points. Each line of the data file represents coordinates  $(x_1, y_1, z_1)$  of a point. Each 3-line segment of the data file performs one major axis. The coordinates are represented in pinion coordinate system  $S_1$ . The applied unit is mm, and the format is **3F22.14**.

**Data File 74:**

This file is designated for drawing of the major axes of contact ellipses,  $M^{(a)}$ , on the gear tooth surface corresponding to the contact points given in data file 42. Each major axis is composed of 3 points. Each line of the data file represents coordinates  $(x_2, y_2, z_2)$  of a point. Each 3-line segment of the data file performs one major axis. The coordinates are represented in gear coordinate system  $S_2$ . The applied unit is mm, and the format is **3F22.14**.

## 7.2 Program 2: Design of Internal Gear Drive

### 7.2.1 Name of the Program

The developed program's name, IGDUIC.FORTRAN, is formed by six characters. The first three characters, IGD, are the initial letters of Internal Gear Drive. The following three characters, UIC, mean that the program is developed at the University of Illinois at Chicago. The program name is easy to remember before the start of computations.

The extension name of the program is FORTRAN. It means that the program is written in standard FORTRAN77 language.

### 7.2.2 Function of the Program

This program is developed to design the internal helical gear drive of double circular-arc teeth. The program includes (1) generation of helical pinion and gear of double circular-arc teeth by rack-cutters, respectively (the gear

is an internal one and pinion is an external one) and (2) tooth contact analysis of contact paths and lower transmission errors. The equations in the program have been represented in Sections 3 and 5.

### 7.2.3 Input Data File 90

Before running the program, you should prepare the following data in data file 90:

Helix angle	$\beta$ (degree)
Diametral pitch	$P_d$ (1/in.)
Number of gear teeth	$N_g$
Number of pinion teeth	$N_p$
Pressure angle	$\alpha$ (degree)
Error of crossing angle	$\Delta\gamma_y$ (degree)
Error of center distance	$\Delta C$ (in.)
Error of intersection angle	$\Delta\gamma_x$ (degree)
Error of gear leader angle	$\Delta\lambda_F$ (degree)
Coefficient of parabolic parameter	$a$

and profile parameters of a rack-cutter in normal section (fig. 25):  $h_a^*$ ,  $c^*$ ,  $\rho_a^*$ ,  $\rho_f^*$ , and  $\Delta e^*$ . Here  $\rho_a = \rho_a^*/P_d$  (or  $\rho_a^*m$ ).

### 7.2.4 Running the Program

The command for running a program in CMS system is as follows:

```
fortvclg IGDUIC <Enter>
```

When you run the program, the following information will appear on the screen:

```
*** WELCOME TO USE IGDUIC ***

END OF READING THE INPUT DATA!

END OF STARTING POINT FOR UPPER CONTACT PATH!

END OF STARTING POINT FOR LOWER CONTACT PATH!

STARTING THE TOOTH CONTACT ANALYSIS!

END OF TCA!

PROGRAM FINISHED!
```

### 7.2.5 Output Data Files

When you finish running the program, IGDUIC, you have completed the design for the internal helical gear drive of double circular arc. All information regarding the output data is listed in several data files. You can open these files and look through them. Detailed information about these output files is given in the following sections:

#### Data File 09:

It includes the input information, pitch radii of gears, and position errors.

**Data File 50:**

It contains transmission errors of one meshing cycle for upper contact path  $M^{(a)}$  (fig. 3). They are obtained by TCA. The format is as follows:

$\phi_{11}$ (degree)	$\Delta\phi_{21}$ (arcsec)
$\phi_{12}$ (degree)	$\Delta\phi_{22}$ (arcsec)
$\phi_{13}$ (degree)	$\Delta\phi_{23}$ (arcsec)
...	...
$\phi_{1_i}$ (degree)	$\Delta\phi_{2_i}$ (arcsec)
...	...

**Data File 60:**

It contains transmission errors of one meshing cycle for lower contact path  $M^{(b)}$  (fig. 3). The format is the same as that in data file 50.

**Data File 61:**

This is the lower contact path  $M^{(b)}$  (fig. 3) represented on the pinion tooth surface. Each line of the data file represents coordinates  $(x_1, y_1, z_1)$  of a contact point of the contact path. The coordinates are represented in pinion coordinate system  $S_1$ . The applied unit is mm, and the format is **3F22.14**.

**Data File 62:**

This is the lower contact path  $M^{(b)}$  (fig. 3) represented on the gear tooth surface. Each line of the data file represents coordinates  $(x_2, y_2, z_2)$  of a contact point of the contact path. The coordinates are represented in gear coordinate system  $S_2$ . The applied unit is mm, and the format is **3F22.14**.

**Data File 51:**

This is the upper contact path  $M^{(a)}$  (fig. 3) represented on the pinion tooth surface. Each line of the data file represents coordinates  $(x_1, y_1, z_1)$  of a contact point of the contact path. The coordinates are represented in pinion coordinate system  $S_1$ . The applied unit is mm, and the format is **3F22.14**.

**Data File 52:**

This is the upper contact path  $M^{(a)}$  (fig. 3) represented on the gear tooth surface. Each line of the data file represents coordinates  $(x_2, y_2, z_2)$  of a contact point of the contact path. The coordinates are represented in gear coordinate system  $S_2$ . The applied unit is mm, and the format is **3F22.14**.

## 7.3 Program 3: Design of Grinding Disk

### 7.3.1 Name of the Program

The developed program's name, DISKUIC.FORTRAN, is formed by seven characters. The first four characters, DISK, mean that the program is used to design a grinding DISK. The following three characters, UIC, mean that program is developed at the University of Illinois at Chicago. The program name is easy to remember before the start of computations.

The extension name of the program is FORTRAN. That means that the program is written in standard FORTRAN77 language.

### 7.3.2 Function of the Program

This program is developed to design a grinding disk for internal or external gear of double circular-arc teeth that is the same as that generated by a rack-cutter. The program includes (1) generation of helical pinion and gear of double circular-arc teeth by rack-cutters, respectively, and (2) design of grinding disk based on gear (pinion) tooth surface. The equations in the program have been represented in Section 4.

### 7.3.3 Input Data File 91

Before running the program, you should prepare the following data in data file 91:

Helix angle	$\beta$ (degree)
Diametral pitch	$P_d$ (1/in.)
Number of gear (pinion) teeth	$N$
Pressure angle	$\alpha$ (degree)

and profile parameters of a rack-cutter in normal section (fig. 25):  $h_a^*$ ,  $c^*$ ,  $\rho_a^*$ ,  $\rho_f^*$ , and  $\Delta e^*$ . Here  $\rho_a = \rho_a^*/P_d$  (or  $\rho_a^*m$ ).

### 7.3.4 Running the Program

The command for running a program in CMS system is as follows:

```
fortvc1g DISKUIC <Enter>
```

When you run the program, the following information will appear on the screen:

```
*** WELCOME TO USE DISKUIC ***
```

```
PITCH RADIUS OF GEAR= 137.84875 (MM)
```

```
PLEASE CHOOSE PITCH RADIUS OF GRINDING DISK? (UNIT:MM)
```

?

Please key in the value and press **Enter**:

```
18 <Enter>
```

Then you will see the following information on the screen:

```
***** PLEASE CHOOSE: *****
```

```
FOR INTERNAL GEAR, PRESS 1 AND <Enter>.
```

```
FOR EXTERNAL GEAR, PRESS 2 AND <Enter>.
```

```
*****
```

?

If you want to get the grinding disk for internal gear, please press **1** and **Enter**:

1 <Enter>

PROGRAM FINISHED!

### 7.3.5 Output Data Files

When you finish running the program, DISKUIC, you have completed the design of the grinding disk. All information regarding the output data is listed in several data files. You can open these files and look through them. Detailed information about these output files is given in the following sections:

#### Data File 09:

It includes the input information and pitch radii of gear and disk.

#### Data File 52 (or 62):

Data file 52 contains axial profile of grinding disk for external gear, and data file 62 contains axial profile of grinding disk for internal gear. The format is as follows (fig. 15):

$z_{t1}$ (mm)	$\rho_{t1}$ (mm)
$z_{t2}$ (mm)	$\rho_{t2}$ (mm)
$z_{t3}$ (mm)	$\rho_{t3}$ (mm)
...	...
$z_{ti}$ (mm)	$\rho_{ti}$ (mm)
...	...

## 7.4 Program 4: Design of Grinding Worm

### 7.4.1 Name of the Program

The developed program's name, WORMUIC.FORTRAN, is formed by seven characters. The first four characters, WORM, mean that the program is to design a grinding WORM. The following three characters, UIC, mean that program is developed at the University of Illinois at Chicago. The program name is easy to remember before the start of computations.

The extension name of the program is FORTRAN. It means that the program is written in standard FORTRAN77 language.

### 7.4.2 Function of the Program

This program is developed to design a grinding worm that generates the modified pinion tooth surface. The program includes (1) thread surface of grinding worm which is generated by rack-cutter P and (2) generation of the modified helical pinion of double circular-arc tooth by the worm. The equations in the program have been represented in Section 6.

### 7.4.3 Input Data File 90

Before running the program, you should prepare the following data in data file 90:

Helix angle	$\beta$ (degree)
Diametral pitch	$P_d$ (1/in.)



Number of gear teeth	$N$
Number of pinion teeth	$N_p^g$
Pressure angle	$\alpha$ (degree)
Error of crossing angle	$\Delta\gamma_y$ (degree)
Error of center distance	$\Delta C$ (in.)
Error of intersection angle	$\Delta\gamma_x$ (degree)
Error of gear leader angle	$\Delta\lambda_F$ (degree)
Coefficient of parabolic parameter	$a$

and profile parameters of a rack-cutter in normal section (fig. 25):  $h_a^*$ ,  $c^*$ ,  $\rho_a^*$ ,  $\rho_f^*$ , and  $\Delta e^*$ . Here  $\rho_a = \rho_a^*/P_d$  (or  $\rho_a^*m$ ).

#### 7.4.4 Running the Program

The command for running a program in CMS system is as follows:

```
fortvclg WORMUIC <Enter>
```

When you run the program, the following information will appear on the screen:

```
*** WELCOME TO USE WORMUIC ***
```

```
END OF WORM DESIGN!
```

```
PROGRAM FINISHED!
```

#### 7.4.5 Output Data Files

When you finish running the program, WORMUIC, you have completed the design of grinding worm. All information about the output data is listed in several data files. You can open these files and look through them. Detailed information about these output files is expressed in the following sections:

##### Data File 09:

It includes the input information, pitch radii of pinion and worm, and lead angle of worm.

##### Data File 42:

Data file 42 contains 21 cross section of worm thread in one circle. There are 100 points for each cross section. Each line of the data file represents three coordinates ( $x_w$ ,  $y_w$ ,  $z_w$ ) of one point and are in worm coordinate system  $S_w$ . The format of data is 3F15.8, and the applied unit is mm.

## References

1. Wildhaber, E.: Helical Gearing U.S. Patent No. 1,601,750, Oct. 5, 1926.
2. Novikov, M.L.: Helical Gearing. USSR Patent No. 109,750, 1956.
3. Litvin, F.L.: Theory of Gearing. First ed. (1960), Second ed. (1968), Nauka (in Russian).
4. Litvin, F.L.: Theory of Gearing. NASA RP-1212 (AVSCOM TR-88-C-035), 1989.
5. Litvin, F.L.: Gear Geometry and Applied Theory. Prentice-Hall, Inc., 1994.
6. Litvin, F.L.; and Lu, J.: Computerized Simulation of Generation, Meshing and Contact of Double Circular-Arc Helical Gears. Mathematical and Computer Modelling, vol. 18, no. 5, June 1993, pp. 31-47.
7. Litvin, F.L.; and Lu, J.: Computerized Design and Generation of Double Circular-Arc Helical Gears With Low Transmission Errors. Computer Methods in Applied Mechanics and Engineering, vol. 127, no. 1-4, 1995, pp. 57-86.
8. Lu, J.; Litvin, F.L.; and Chen, J.S.: Load Share and Finite Element Stress Analysis for Double Circular-Arc Helical Gears. Mathematical and Computer Modelling, vol. 21, no. 10, 1995, pp. 13-30.

<b>REPORT DOCUMENTATION PAGE</b>			Form Approved OMB No. 0704-0188		
Public reporting burden for this collection of information is estimated to average 1 hour per response, including the time for reviewing instructions, searching existing data sources, gathering and maintaining the data needed, and completing and reviewing the collection of information. Send comments regarding this burden estimate or any other aspect of this collection of information, including suggestions for reducing this burden, to Washington Headquarters Services, Directorate for Information Operations and Reports, 1215 Jefferson Davis Highway, Suite 1204, Arlington, VA 22202-4302, and to the Office of Management and Budget, Paperwork Reduction Project (0704-0188), Washington, DC 20503.					
<b>1. AGENCY USE ONLY (Leave blank)</b>		<b>2. REPORT DATE</b> July 1997	<b>3. REPORT TYPE AND DATES COVERED</b> Final Contractor Report		
<b>4. TITLE AND SUBTITLE</b>  New Methods for Improved Double Circular-Arc Helical Gears			<b>5. FUNDING NUMBERS</b>  WU-581-30-13 1L161102AH45		
<b>6. AUTHOR(S)</b>  Faydor L. Litvin and Jian Lu					
<b>7. PERFORMING ORGANIZATION NAME(S) AND ADDRESS(ES)</b>  University of Illinois at Chicago Chicago, Illinois 60680			<b>8. PERFORMING ORGANIZATION REPORT NUMBER</b>  E-10701		
<b>9. SPONSORING/MONITORING AGENCY NAME(S) AND ADDRESS(ES)</b>  U.S. Army Research Laboratory Cleveland, Ohio 44135-3191 and NASA Lewis Research Center Cleveland, Ohio 44135-3191			<b>10. SPONSORING/MONITORING AGENCY REPORT NUMBER</b>  NASA CR-4771 ARL-CR-339		
<b>11. SUPPLEMENTARY NOTES</b>  Project Manager, Dennis P. Townsend, Structures and Acoustics Division, NASA Lewis Research Center, organization code 5950, (216) 433-3955.					
<b>12a. DISTRIBUTION/AVAILABILITY STATEMENT</b>  Unclassified - Unlimited Subject Category 37  This publication is available from the NASA Center for AeroSpace Information, (301) 621-0390.			<b>12b. DISTRIBUTION CODE</b>		
<b>13. ABSTRACT (Maximum 200 words)</b>  The authors have extended the application of double circular-arc helical gears for internal gear drives. The geometry of the pinion and gear tooth surfaces has been determined. The influence of errors of alignment on the transmission errors and the shift of the bearing contact have been investigated. Application of a predesigned parabolic function for the reduction of transmission errors was proposed. Methods of grinding of the pinion-gear tooth surfaces by a disk-shaped tool and a grinding worm were proposed.					
<b>14. SUBJECT TERMS</b>  Gear; Geometry; Low noise; Double circular arc; Helical; Computerized; Simulation			<b>15. NUMBER OF PAGES</b> 58		
			<b>16. PRICE CODE</b> A04		
<b>17. SECURITY CLASSIFICATION OF REPORT</b> Unclassified	<b>18. SECURITY CLASSIFICATION OF THIS PAGE</b> Unclassified	<b>19. SECURITY CLASSIFICATION OF ABSTRACT</b>	<b>20. LIMITATION OF ABSTRACT</b>		



